



Chitosan encapsulated S-nitrosoglutathione is an efficient nanodonor in *Brassica napus* seedlings

Dóra Kondak ^a , Ágota Deák ^b, Andrea Rónavári ^c , Tamás Bodor ^{a,d}, Selahattin Kondak ^a , Oluwatosin Peace Adedokun ^a, Péter Benkő ^e , Réka Szöllősi ^a, Gabriella Szalai ^f, Tibor Janda ^f , Ferhan Ayaydin ^{g,h}, Christian Lindermayr ⁱ, Zoltán Kónya ^c , Zsuzsanna Kolbert ^{a,*}

^a Department of Plant Biology, University of Szeged, Közép Fásor 52., H6726 Szeged, Hungary

^b Department of Physical Chemistry and Materials Science, University of Szeged, Rerrich Béla Tér 1., H6720 Szeged, Hungary

^c Department of Applied and Environmental Chemistry, University of Szeged, Rerrich Béla Tér 1., H6720 Szeged, Hungary

^d Doctoral School of Biology, Faculty of Science and Informatics, University of Szeged, Közép Fásor 52., H6726 Szeged, Hungary

^e HUN-REN Biological Research Centre, Temesvári Krt. 62., H6726 Szeged, Hungary

^f HUN-REN Centre for Agricultural Research, Martonvásár, Brunszvik U. 2., H2462 Szeged, Hungary

^g Hungarian Centre of Excellence for Molecular Medicine, Functional Cell Biology and Immunology Advanced Core Facility, Budapesti út 9., H6728 Szeged, Hungary

^h Agribiotechnology and Precision Breeding for Food Security National Laboratory, Institute of Plant Biology, HUN-REN Biological Research Centre, 62 Temesvári Krt., Szeged, H-6726, Hungary

ⁱ Institute of Lung Health and Immunity, Helmholtz Zentrum München – German Research Center for Environmental Health, 85764 Munich/Neuherberg, Germany

ARTICLE INFO

Handling Editor: Shivendra Sahi

Keywords:

Nitric oxide delivery
Nanoparticles
Reactive nitrogen species
S-nitrosothiol signaling

ABSTRACT

Nitric oxide (NO) supplementation promotes plant development and stress endurance. To overcome the stability and toxicity issues of conventional NO donors, nanoencapsulation may offer a solution. This study used a model system in which 5-day-old *Brassica napus* L. seedlings were exposed via their root system for 2 h with either bulk S-nitrosoglutathione (GSNO), chitosan-encapsulated GSNO nanoparticles (GSNO-CHT NPs), or empty chitosan nanoparticles (CHT NPs), at concentrations of 250 and 500 μ M. Nanoparticle-associated cell wall modifications of the seedlings' roots and rhizosphere acidification was observed. Fluorescein isothiocyanate (FITC) labelled GSNO-CHT NPs revealed that the internalization of GSNO-CHT-FITC NPs into plant roots was significantly less efficient than that of CHT-FITC NPs. Nano GSNO overperformed bulk GSNO in regards of the intensity and sustainability of *in vitro* NO release, the rate of *in planta* NO accumulation and induction of S-nitrosothiol (SNO) signalling (SNO levels, nitrite levels, *BnNIA1* expression). The GSNO reductase was not activated and the GSNO levels were reduced less by nano NO donor compared to the bulk from. Bulk GSNO-triggered accumulation of free cysteine suggests stress-state of the seedlings in contrast to the milder effect of GSNO-CHT NPs. Additionally, encapsulation of GSNO prevented nitrosative stress induction due to the lack of peroxynitrite induction and slightly increasing protein tyrosine nitration, while bulk GSNO proved to be pronitric in the seedlings. By exploring the interaction between GSNO-CHT NPs and plants from multiple angles for the first time, this study demonstrates the efficacy of GSNO-CHT NPs as an effective, controlled, non-toxic NO donor for plants.

1. Introduction

Nitric oxide and its derivatives, the reactive nitrogen species (RNS) play a fundamental role in physiological processes, ranging from seed and pollen germination, root system development, and flowering, to their roles in responses to biotic (e.g., viruses, bacteria, and fungal pathogens) and abiotic (e.g., drought, temperature, UV light, heavy

metals, hypoxia) stresses (Kolbert et al., 2019).

Plants are in contact with environmental NO being present in the soils and atmosphere due to natural and anthropogenic sources (Ma et al., 2020). Additionally, plants utilize various enzymatic and non-enzymatic, oxidative and reductive pathways for endogenous NO production. The reduction of nitrite to NO catalysed by nitrate reductase (NR) enzyme (Rockel et al., 2002; Mohn et al., 2019) is a relevant

* Corresponding author.

E-mail address: ordogne.kolbert.zsuzsanna@szte.hu (Z. Kolbert).

<https://doi.org/10.1016/j.plaphy.2025.110184>

Received 21 April 2025; Received in revised form 17 June 2025; Accepted 19 June 2025

Available online 20 June 2025

0981-9428/© 2025 The Authors. Published by Elsevier Masson SAS. This is an open access article under the CC BY-NC-ND license (<http://creativecommons.org/licenses/by-nc-nd/4.0/>).

contributor to the NO formation in the root; however, some earlier findings in *Chlamydomonas* suggest that NR indirectly contributes to NO biosynthesis, through mediating the electron transfer to the NO-forming nitrite reductase enzyme (Chamizo-Ampudia et al., 2017). Recently, NO formation in a peroxidase-catalysed reaction from oximes and flavins has been proposed in higher plants (López-Gómez et al., 2024). More recently, peroxisomal sulfite oxidase has been identified as a source of NO in the presence of nitrate and NADH in pepper (Corpas et al., 2025).

At the site of its production due to diverse pathways, NO can react with various molecules, such as reactive oxygen species (ROS), including hydrogen peroxide (H₂O₂) and superoxide radical (O₂^{•-}), metals, and lipids, forming RNS or their derivatives such as *S*-nitrosoglutathione and peroxyxynitrite (ONOO⁻) (Begara-Morales et al., 2018). NO/RNS-associated posttranslational modifications (PTMs) contribute to the formation of molecules like *S*-nitrosothiols or 3-nitrotyrosine, which are involved in signal transduction processes or the development of nitro-oxidative stress. In plants, the central molecule in nitration is ONOO⁻, which arises from the rapid reaction between NO and O₂^{•-} (León, 2022). Nitration in plant proteins is supposed to cause functional loss leading to their proteosomal degradation (Kolbert et al., 2017). *S*-nitrosation refers to the reversible modification of the sulfhydryl (SH) group of a susceptible cysteine amino acid yielding SNOs (Gupta et al., 2020). A representative SNO is GSNO, which is formed via *S*-nitrosation of the cysteine thiol group in the tripeptide glutathione (GSH). GSNO has a half-life of the order of hours and its homolytic cleavage liberates NO (Dent and DeMartino, 2023) and such properties contribute to GSNO being a good candidate for orchestrating the long-distance (e.g., root-shoot) translocation of the NO signal (Kolbert et al., 2024). The level of GSNO is tightly regulated by the function of NADH-dependent GSNO reductase (GSNOR) (Sakamoto et al., 2002), NADPH-dependent thioredoxin reductase (Kneeshaw et al., 2014) and NADPH-dependent aldo-keto reductase (Treffon et al., 2021). Alongside GSNOR, phyto-globins also regulate local GSNO/NO levels by oxidizing NO to nitrate (Meilhoc et al., 2011).

Due to its relative stability under controlled conditions and its capacity to release NO, GSNO is widely used as an exogenous NO donor to enhance stress tolerance in plants (e.g., Methela et al., 2023a; Saini et al., 2024; Khan, 2024). However, in practical applications, especially *in planta* or in open environments, GSNO is prone to rapid degradation due to its sensitivity to light, pH, temperature, and enzymatic breakdown, which limits its effective NO delivery and consistency. To overcome these challenges, polymer-based nanodonor provides an excellent alternative for the enhancement of NO delivery in plant systems. Nanoparticles are chemically diverse molecules, which share the common property that at least one of their dimensions is less than 100 nm (Szöllösi et al., 2020). The encapsulation in a nanochitosan matrix promotes sustained and localized NO release, higher stability and improved bioavailability for the NO donor (Cardozo et al., 2014; Seabra et al., 2022). The advantages of CHT include biodegradability, biocompatibility and antibacterial properties (Xin et al., 2017).

The effects of GSNO-CHT on plants have already been explored in a few experimental setups, but these works don't focus on studying the fate of the nanocapsule and the *in planta* NO/RNS signalling. CHT-encapsulated GSNO nanodonor alleviated the negative effects of water deficit on plant metabolism and increased biomass allocation to the root system in drought-stressed sugarcane (*Saccharum officinarum*) (Silveira et al., 2019). The beneficial effects of GSNO-CHT nanoparticles supplementation on the storability and antioxidant systems of sweet cherry (*Prunus avium*) during cold storage has also been proposed (Ma et al., 2019).

The aim of our work is to gain a deeper understanding of the effect of the CHT-encapsulated GSNO nanodonor on endogenous NO/RNS metabolism and signalling and to better understand the relationship between exogenous NO supply and endogenous NO signalling.

2. Materials and methods

2.1. Synthesis of CHT NPs, GSNO-CHT NPs and free GSNO

The low molecular weight of chitosan (obtained from Sigma-Aldrich, Cat. No. 417963) was used for the synthesis of chitosan nanoparticles. Chitosan was mixed using magnetic stirring in an aqueous solution of 1 % (w/v) acetic acid for overnight to obtain a 10 mg mL⁻¹ CHT solution. Then, the homogeneous CHT solution was diluted 2 fold (resulting in a final concentration of 5 mg mL⁻¹ of CHT) and the pH was set from 3.4 to 4.6 by adding a 10 mol L⁻¹ sodium hydroxide solution. An aqueous sodium tripolyphosphate (TPP, from Sigma-Aldrich) solution (0.25 % (w/v) was added dropwise to the CHT suspension in a volumetric proportion of 3CHT:1TPP. The final mixture was stirred further for 45 min at room temperature, which allows the formation of the aqueous suspension of CHT NPs.

The GSNO containing chitosan nanoparticles were prepared following the same steps as for the synthesis of CHT NPs. The GSH was mixed to the homogeneous CHT solution (5 mg mL⁻¹ of CHT) and after 15 min of stirring an equimolar amount of sodium nitrite (NaNO₂) was added to the suspension. After 15 min of stirring, the TPP solution (0.25 % w/v) was added dropwise (under continuous stirring) to the GSNO-CHT suspension. Then final mixture of GSNO-CHT NPs dispersion was stirred further for 45 min at room temperature.

Free GSNO was synthesized by using GSH (obtained from Sigma-Aldrich) and sodium nitrite (obtained from Sigma-Aldrich) precursors. 50 mM of GSH was reacted with an equimolar amount of NaNO₂ following the equation in Fig. 1B. The synthesized GSNO was characterized by using UV-Vis spectrophotometry.

2.1.1. Encapsulation efficiency of the GSNO-CHT NPs

To determine the encapsulation efficiency (EE%) the absorbance spectra of the supernatants of the centrifuged drug-loaded GSNO-CHT NPs conjugates were registered by Shimadzu UV-1800 UV-vis double beam spectrophotometer in a 1 cm quartz cuvette. The measurements were carried out at room temperature in 200–800 nm wavelength range. The exact concentration of the non-encapsulated free GSNO was calculated from the calibration curve, where the characteristic absorbance band of the GSNO was appeared at $\lambda = 336$ nm in distilled water medium. Encapsulated form of GSNO into the CHT NPs was prepared by using precipitation method adding TPP. The product was collected by centrifugation (Hermle centrifuge Z 36 HK, 14500 g × 20 min), then washed with water and lyophilized.

The encapsulation efficiency of GSNO loaded to CHT NPs was calculated by using Eq. (1):

$$\text{Encapsulation efficiency} = \frac{\text{amount of drug in nanoparticles}}{\text{the total amount of drug added}} \times 100 \quad (1)$$

where the amount of the drug in nanoparticles was calculated from the drug concentration of supernatant measured by UV-spectroscopy.

2.2. Fourier transform infrared (FTIR) measurements

To characterize the obtained CHT NPs, GSNO and GSNO containing CHT NPs FTIR spectroscopy measurements were carried out in the range of 4000 and 500 cm⁻¹ through the accumulation of 128 scans at 1 cm⁻¹ resolution utilizing the BioRad FTS-60A FTIR spectrometer. Thermo Scientific GRAMS/AI Suite software was used for all spectral analyses.

2.3. Dynamic light scattering (DLS) studies

The average size, size distribution and polydispersity index of the CHT NPs and GSNO-CHT NPs were measured by dynamic light scattering (DLS) using a HORIBA SZ-100 NanoParticle Analyzer (Retsch Technology GmbH, Germany) at room temperature. The light source

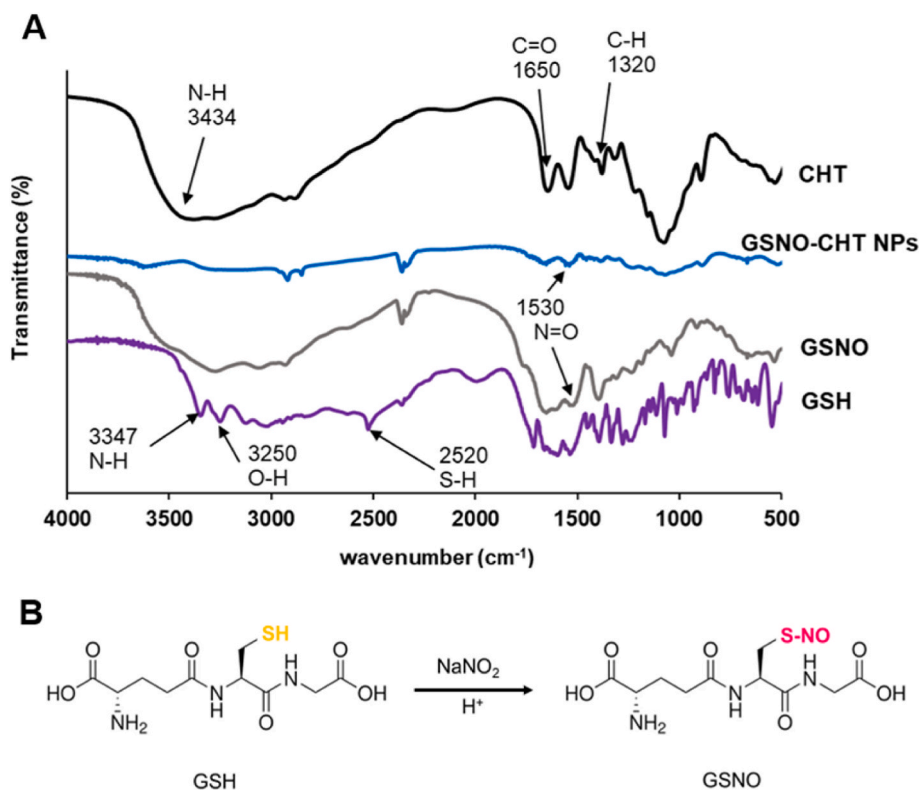


Fig. 1. (A) FTIR spectra of pure CHT, GSNO-CHT NPs, GSNO and pure GSH. (B) Equation of the reaction between GSH and NaNO₂ to form GSNO.

was a semiconductor laser ($\lambda = 532$ nm, 10 mW) and photomultiplier tubes (PMT) were used as detector at 90° scattering angle. The particle size distribution was calculated using the cumulant method, then the histogram method was applied to obtain the mean and the standard deviation of the distribution function from the average of 10 separate measurements from each sample.

2.4. TEM measurements

A transmission electron microscope (TEM) was utilized to examine the particle size and the morphology of prepared CHT NPs and GSNO-CHT NPs. The analysis was performed on a FEI TECNAI G² 20 X-Twin high-resolution transmission electron microscope with a 200 kV acceleration voltage. The samples were dispersed in distilled water then droplets were dried on a copper-mounted carbon film (200 mesh) for TEM measurements.

2.5. Plant material, growing conditions and nanomaterial treatment

Canola (*Brassica napus* L. cv. GK Gabriella) seeds underwent surface sterilization, which involved a 1-min treatment with 70 % ethanol followed by a 15-min exposure to 5 % sodium hypochlorite and 5 times washing with distilled water. Subsequently, the seeds were placed in 9 cm diameter Petri dishes containing wet filter paper. The Petri dishes were positioned in a controlled environment for 5 days (a photon flux density of 150 $\mu\text{mol m}^{-2} \text{s}^{-1}$, a 12-h light/12-h dark cycle, relative humidity ranging between 55 % and 60 %, and a temperature maintained at 24 ± 2 °C).

Freshly prepared 50 mM GSNO, GSNO-CHT, and CHT suspensions (pH 4.6) were diluted with distilled water to achieve concentrations of 250, 500, 750, and 1000 μM . On the day of sampling, treatments were applied for 0.5, 1, 2, 3, 4, and 5 h. Filter papers were wetted either with 10 mL of distilled water (Control) or with an equal volume of nanoparticle suspensions.

2.6. Spectrofluorometric determination of fluorescein isothiocyanate (FITC) labelling

The absorption-emission spectra of FITC, GSNO-CHT-FITC, CHT-FITC suspensions were recorded by a spectrofluorometer (Hitachi F-4500, Hitachi Ltd., Tokyo, Japan) in a wavelength scan mode. A solution of FITC (0.08 mg mL⁻¹) was diluted with distilled water to a concentration of 0.002 nM (2 mL final volume). The 50 mM stocks of GSNO-CHT-FITC and CHT-FITC solutions were diluted with distilled water to 0.002 nM (2 mL final volume). Excitation (exc.) maxima was recorded at ~488 nm and maximum emission (em.) was recorded at ~515 nm. The spectra are presented as Fig. S1.

2.7. Confocal microscopic examination of nanocapsule internalization

For studying the *in planta* presence of the nanocapsules, we used FITC-conjugated GSNO-CHT and CHT nanomaterials at concentrations of 500 μM . The FITC-containing GSNO-CHT NPs and CHT NPs were prepared using the same steps as those for synthesizing the GSNO-CHT NPs and CHT NPs. For GSNO-CHT-FITC, GSH and FITC was added to the homogeneous CHT solution (5 mg mL⁻¹ of CHT) at pH of 4.6. The concentration of the a GSH was 50 mM and an equimolar amount of NaNO₂ was added to the suspension. After 15 min of stirring, the TPP solution (0.25 % w/v) was added dropwise (under continuous stirring) to the GSNO-CHT-FITC NPs dispersion. The final mixture of GSH-CHT NPs dispersion was stirred further for 45 min at room temperature. In the nanoparticle suspensions, the concentration of FITC was 0.482 $\mu\text{g mL}^{-1}$ (in case of 100 % bound). Besides GSNO-CHT-FITC and CHT-FITC, distilled water, free FITC (0.241 $\mu\text{g mL}^{-1}$ concentration), GSNO, GSNO-CHT and CHT-treated samples were used as Controls. After treatments (2 h), root samples were examined with Leica Stellaris 5 confocal laser scanning microscope using HC PL FLUOTAR 10x (N.A. 0.30) and HC PL APO 20x (N.A. 0.75) dry objectives. Tunable white light laser was set to 495 nm excitation and FITC emission was detected between 501 nm and 595 nm. Bright field image was captured with transmitted light detector.

2.8. Visualization of root cell wall components, including lignin, callose and pectin

Ruthenium Red (RR) was employed to observe the pectin content in the root tips, using the method outlined by Durand et al. (2009). Root samples were immersed in a 0.05 % (w/v) RR solution for 15 min, rinsed with distilled water, and mounted on slides.

To visualize the level of lignin in the roots, phloroglucinol-HCl solution was employed. The roots were immersed in a 1 % (w/v) phloroglucinol solution that had been prepared in 6 N HCl for 5 min. Afterward, they were rinsed with distilled water and mounted on slides, following the method described by Rogers et al. (2005).

For callose detection, root tips were submerged in an aniline blue solution (0.1 % aniline blue (w/v) and 1 M glycine, dissolved in distilled water) for 5 min at room temperature in the dark, then rinsed once in distilled water (Cao et al., 2011).

2.9. Visualization of changes in rhizosphere pH

The visualization of rhizosphere acidification was conducted under greenhouse lighting (a photon flux density of $150 \mu\text{mol m}^{-2} \text{s}^{-1}$, a 12-h light/12-h dark cycle), for 2 h with the following treatments: Control (with and without water), 250 and 500 μM GSNO, GSNO-CHT, and CHT solutions. The agar medium consisted of 0.75 % (w/v) agar, 0.006 % (w/v) bromocresol purple, 2.5 mM K_2SO_4 , and 1 mM CaSO_4 , with the pH adjusted to 6. The roots of 5-day-old seedlings were gently embedded in the agar to avoid any damage (Yan et al., 2001). For each treatment, a medium was prepared without plants, and the treatment solutions were applied on the surface of the agar media as drip along a vertical line, in order to isolate the effect of the treatment solutions from acidification. Petri dishes were photographed under white transillumination (Dark Hood DH-50, Biostep, Germany) using a Canon EOS 700D camera (Tokyo, Japan). Pixel density was quantified with the ImageJ software.

2.10. Electrochemical detection of in vitro NO release

The NO-sensitive electrode (ISO-NOP, 2 mm, World Precision Instruments Inc., Sarasota, FL, USA) was calibrated using a method based on *S*-nitroso-*N*-acetylpenicillamine (SNAP) decomposition to NO in the presence of copper (Zhang, 2004). One mL of GSNO, GSNO-CHT and CHT (250 or 500 μM concentration) were measured immediately after preparation. To ensure constant mixing of the solution a magnetic stirrer was applied during the measurement. The measurements were done at room temperature and under $100\text{--}200 \mu\text{mol m}^{-2} \text{s}^{-1}$ illumination. NO concentration (nM) was calculated from a standard curve.

2.11. Detection of in planta RNS and ROS levels using fluorescence microscopy

Semi-quantitative assessment of NO, ONOO⁻ levels were performed in root tips, mature root zones, handmade cross sections from hypocotyls and cotyledons of *B. napus* seedlings. Due to technical issues, the detection of H₂O₂ was done in the root tips and hypocotyl sections, and O₂^{•-} was visualized only in the roots.

For studying NO, samples were incubated in a solution of 10 μM 4-amino-5-methylamino-2',7'-difluorofluorescein diacetate (DAF-FM DA) fluorescent probe. The staining solution was prepared in a 10 mM TRIS-HCl buffer with a pH of 7.4. The samples were incubated in darkness at room temperature for 30 min. Subsequently, the samples were washed twice with the buffer and mounted on microscopic slides (Kolbert et al., 2012).

Aminophenyl fluorescein (APF) at a concentration of 10 μM was employed to detect ONOO⁻ levels. The samples were subjected to incubation with this probe for 1 h at room temperature in the absence of light. Subsequently, they were washed twice with 5 mM TRIS-HCl buffer (pH 7.4) before being subjected to microscopic analysis (Kolbert et al.,

2012).

Samples were submerged in a solution containing 50 μM of 10-acetyl-3,7 dihydroxyphenoxazine (Amplex Red) prepared in 50 mM sodium phosphate buffer with a pH of 7.5. This solution was used to label H₂O₂ levels. After a 30-min incubation period at room temperature in the absence of light, the seedlings were rinsed in 50 mM sodium phosphate buffer (pH of 7.5) and then positioned on microscopic slides (Lehotai et al., 2012).

Dihydroethidium (DHE) was utilized to detect superoxide (O₂^{•-}) levels. Samples were stained with a 10 μM DHE solution prepared in 10 mM Tris-HCl buffer (pH 7.4). Samples were incubated in the dye solution at 37 °C in the dark for half an hour, then washed them twice with Tris-HCl buffer before placing them on the slide (Kolbert et al., 2012).

All analyses were performed using Zeiss Axiovert 200M fluorescent microscope (Carl Zeiss, Jena, Germany) equipped with digital camera (Axiocam HR) and 10 × (root and cotyledon samples) or 5 × (hypocotyl samples) objectives. Filter set 10 (exc.: 450–490, em.: 515–565 nm) was used for DAF-FM and APF. Filter set 9 (exc.:450–490 nm, em.:515–∞ nm) for DHE, Filter set 20 (exc.: ~540, em.: ~590 nm) for Amplex Red and DAPI filter set (exc.: 365, em.: 430–480 nm) for aniline blue. Lignin and pectin staining was detected using transmitted light imaging. Axiovision Rel. 4.8 software (Carl Zeiss, Jena, Germany) was used to measure pixel intensities (diameter of circles in the area of which the pixel intensities were measured: 116 μm [root tip], 466 μm [hypocotyl], 266 μm [cotyledon]) on digital photographs. This analysis was carried out at least three times with 10 root tips examined (n = 10).

2.12. Gene expression analysis by RT-qPCR

Root and shoot samples of *B. napus*, previously frozen at $-80 \text{ }^\circ\text{C}$, were ground in liquid nitrogen, followed by RNA extraction using the Quick-RNA Miniprep Kit (Zymo Research, Irvine, CA, USA) in accordance with the manufacturer's instructions. The quality and quantity of the isolated RNA were evaluated using a NanoDrop™ 2000/2000c spectrophotometer (Thermo Fisher Scientific, Waltham, MA, USA).

For cDNA synthesis 1 μg of total RNA was reverse-transcribed into cDNA using the RevertAid First Strand cDNA Synthesis Kit (Thermo Fisher Scientific) according to the manufacturer's instructions. Primers were designed with the NCBI primer design tool (Ye et al., 2012). Primer sequences are listed in Table S1. Quantitative Real time PCR (qRT-PCR) was performed on the CFX384 Touch Real-Time PCR Detection System (Bio-Rad Laboratories Inc., Hercules, CA, USA) using a 1:10 dilution of cDNA to assess relative mRNA levels. BnActin7 (Bra028615) was used as the reference gene. RT-qPCR reactions were conducted in a total volume of 7 μL . The PCR mixture included 1 μL cDNA, 0.21 μL each of forward and reverse primers, and 3.5 μL Maxima SYBR Green/ROX qPCR Master Mix (2x) (Thermo Fisher Scientific). The reaction mix was aliquoted into Hard-Shell® 384-well plates (thin-wall, skirted, white; Bio-Rad, Cat. no: HSP3805). The amplification process followed a standard two-step thermal cycling profile: 10 s at 95 °C and 1 min at 60 °C for 40 cycles, after a 15-min preheating step at 95 °C. A dissociation stage was then added, consisting of 95 °C for 15 s, 60 °C for 15 s, and 95 °C for 15 s. Data analysis was performed using Bio-Rad CFX Maestro software and Microsoft Excel 2019, with relative mRNA levels calculated by the $2^{-\Delta\Delta\text{Ct}}$ method.

2.13. SNO and nitrite quantification

The total amount of SNO was quantified by Sievers 280i NO analyzer (GE Analytical Instruments, Boulder, CO, USA). *B. napus* seedlings were grinded in liquid nitrogen and 250 mg of the powder was mixed with one volume of 1 × PBS buffer (137 mM NaCl, 4.3 mM Na₂HPO₄, 2.7 mM KCl and 2.47 mM KH₂PO₄ including 10 mM N-ethylmaleimide and 2.5 mM EDTA, pH 7.4). Samples were centrifuged twice for 15 min at 20,000 ×g at 4 °C each. For nitrite measurements, 100 μl of each sample was into the reaction vessel filled with potassium iodide – each sample

was measured two times. For SNO measurements, the supernatants were incubated with 32 mM sulfanilamide (prepared in 1 M HCl) at a ratio of 9:1 in order to remove nitrite. Of each sample 200 μ l was injected – each sample was measured three times. Nitrite and SNO concentrations were quantified with the help of NO analysis software (v3.2) by integrating peak areas and using a standard curve. The standard curve was generated by adding known concentrations of sodium nitrite. These experiments were carried out on three separate plant generations with five samples examined each ($n = 5$).

2.14. Analysis of tyrosine nitration by Western blot

To extract proteins, *B. napus* seedlings were ground using a 50 mM TRIS-HCl extraction buffer with a pH of 7.6–7.8. The protein extract was then subjected to centrifugation at 4 °C, at 9300 \times g for 20 min. Subsequently, the protein extract was treated with a 1 % proteinase inhibitor (Sigma-Aldrich, Cat. No.: P9599, St. Louis, Missouri, USA) and stored at –20 °C. Protein concentrations were determined using bovine serum albumin as a standard (Bradford, 1976).

For SDS-PAGE analysis, 15 μ l of protein sample was denatured by mixing with buffer (62.5 mM Tris-HCl (pH 6.8), 2 % (w/v) SDS, 10 % (v/v) glycerol, 0.01 % (w/v) bromophenol blue, and 100 mM DTT) and incubating at 95 °C for 5 min. This step ensures complete protein denaturation by disrupting secondary and tertiary structures, and reducing disulfide bonds. SDS imparts a uniform negative charge to the proteins, enabling their separation solely based on molecular weight during electrophoresis. The proteins were subsequently transferred to PVDF membranes using the wet blotting procedure, employing a constant current of 25 mA for 16 h. To prevent non-specific antibody binding in the detection of protein tyrosine nitration, membranes were blocked in 5 % (w/v) non-fat dry milk prepared in TBST buffer (20 mM Tris, 178 mM NaCl, 0.05 % Triton X-100, pH 7.8). Membranes were employed for cross-activity assays using a rabbit polyclonal antibody against 3-nitrotyrosine (diluted at 1:2000, Sigma-Aldrich, Cat. No.: N0409, St. Louis, Missouri, USA) was employed. Immunodetection was carried out using an affinity-isolated goat anti-rabbit IgG alkaline phosphatase secondary antibody (Sigma-Aldrich, Cat. No. A3687, diluted at 1:10,000). The protein bands were visualized using the NBT/BCIP (5-bromo-4-chloro-3-indolyl phosphate) reaction. Nitrate bovine serum albumin (NO₂-BSA) from Sigma-Aldrich (Cat No. A3653) was utilized as a positive Control (Kolbert et al., 2018). Protein bands were quantified by utilizing Gelquant software (provided by [biochemlabsolutions.com](https://www.biochemlabsolutions.com)), and the results were expressed as pixel densities. Western blot analysis was conducted on three separate protein extracts from independent plant generations, with at least two analyses performed for each extract.

2.15. Assessment of GSNOR activity using UV–visible absorption spectroscopy

The activity of GSNOR in whole seedling extracts was measured spectrophotometrically by monitoring NADH consumption in the presence of GSNO, as described in detail below. GSNOR activity was determined by monitoring the oxidation of NADH in the presence of GSNO at 340 nm, following the method outlined by Sakamoto et al. (2002). A KONTRON UVikon double-beam spectrophotometer was used for this purpose. Fresh plant material weighing 250 mg was ground with an extraction buffer composed of 100 mM TRIS-HCl (pH 7.5), 10 % (w/v) glycerol, 0.2 % (w/v) Triton-X, 2 mM DTT, and 0.1 mM EDTA. The resulting homogenate was centrifuged at 9300 \times g for 20 min at 4 °C. Subsequently, 150 μ l of the protein extract was incubated in a mixture consisting of 650 μ l reaction buffer (20 mM TRIS-HCl pH 8.0, 0.5 mM EDTA), 100 μ l of 0.2 mM NADH, and 100 μ l of 0.4 mM GSNO. The protein concentration was determined using the Bradford protein assay (Bradford, 1976). The GSNOR activity data were expressed as nmol mg⁻¹ protein. The measurement of GSNOR activity was performed in

three separate generations of plants, with three technical replicates for each ($n = 3$).

2.16. GSNO immunohistochemistry

The detection of GSNO in plant tissues was carried out by performing immunohistochemical analysis on cross sections obtained from the primary root, hypocotyl, and cotyledon. The preparation of these sections followed the general protocol described by Barroso et al. (2006), with necessary adaptations. Initially, tissue samples were fixed by immersing them in a 4 % (w/v) paraformaldehyde solution, which helps to preserve cellular structures and antigenicity. After fixation, samples were thoroughly rinsed with distilled water to remove excess fixative and prepare the tissues for embedding. Subsequently, the tissues were embedded in a 5 % (w/v) bacterial agar matrix. This step was based on the method of Zelko et al. (2012), with slight modifications to accommodate the sample type and experimental setup. Once embedded, the tissues were sectioned into uniform 100 μ m thick slices using a vibratome (Zeiss-Microm, HM650V), allowing for consistent and reproducible analysis across samples. For immunolabeling, the sections were incubated overnight at 4–8 °C with a 1:2500 dilution of rat anti-GSNO antibody (VWR Chemicals, Poole, England). The antibody was prepared in TBSA-BSAT solution, which consisted of 5 mM Tris, 9 % (w/v) NaCl, 0.05 % (w/v) sodium azide, 0.1 % (w/v) bovine serum albumin (BSA), and 0.1 % (w/v) Triton X-100, with the pH adjusted to 7.2. This buffer composition ensured optimal antibody stability and tissue permeability during the incubation. Following primary antibody incubation, the sections were washed three times with the same buffer to remove unbound antibodies. Afterward, a secondary antibody—anti-rat IgG conjugated with fluorescein isothiocyanate (FITC) (Agrisera, Vännäs, Sweden)—was applied at a 1:1000 dilution, in accordance with the method described by Corpas et al. (2008). This allowed for specific detection of GSNO-associated fluorescence. For visualization, the labelled tissue sections were mounted on microscope slides using a 1:1 mixture of phosphate-buffered saline (PBS) and glycerine. Fluorescence imaging was conducted using a Zeiss Axiovert 200M fluorescence microscope equipped with Filter Set 10. Objective magnifications were selected based on tissue type: 40 \times for primary root sections, 10 \times for hypocotyl sections, and 5 \times for cotyledon sections, allowing for optimal visualization of the fluorescence signal across different tissue structures. All immunohistochemical analyses were performed on two independent biological replicates, with four technical replicates per sample to ensure reproducibility and reliability of the results.

2.17. Analysis of cys and cys-containing metabolites

For determination of thiols (reduced and oxidized form of cysteine, γ -glutamylcysteine and glutathione) 0.2 g plant material was ground in liquid nitrogen in a mortar with a pestle and extracted with 1 ml 0.1 M HCl. After centrifugation (10,000 g, 10 min, 4 °C) for measurement of total thiols 120 μ l supernatant was added to a mixture containing 180 μ l CHES buffer (pH 9.3) and 30 μ l 3 mM dithiothreitol and kept at room temperature for 60 min for reduction of thiols. For labelling 20 μ l 15 mM monobromobimane was added. After 15 min at room temperature in the dark the reaction was stopped with 250 μ l 0.25 % methanesulfonic acid. In parallel for measurement of oxidized thiols 30 μ l 50 mM N-ethylmaleimide (NEM) was added to the mixture of 400 μ l supernatant and 600 μ l CHES buffer (pH 9.3) for blocking the reduced thiols. The reaction time was 15 min at room temperature. The excess NEM was removed with extraction three times with equal volume of toluene. 300 μ l NEM treated extract was reduced and labelled as described above.

After membrane filtration (teflon, 0.45 μ m pore size) thiols were separated on a HyperPrep HS BDS C18 column (250 \times 4.6 mm, particle size 8 μ m; ThermoScientific, Waltham, MA, USA) using a W2690 (Waters, Milford, MA, USA) separation module. Solvents: A: 10 % HPLC grade methanol containing 0.25 % acetic acid (pH 3.9); B: 90 % HPLC grade

methanol containing 0.25 % acetic acid. Gradient (%B): 1 min: 0 %; 10 min: 8 %; 15 min: 14 %; 17.5 min: 100 %; 25.5 min: 100 %; 26.5 min 0 %; 31 min: 0 %. Compounds were detected using a W2475 (Waters, Milford, MA, USA) scanning fluorescence detector (ex.: 380 nm; em.: 480 nm). Compounds were quantified using external calibration curves.

2.18. Statistical analysis

The results are presented as mean \pm standard error (SE). Graphs were created using Microsoft Excel 2016 and SigmaPlot 12. Statistical analysis was performed using the Duncan test (one-way ANOVA, significance level set at $P < 0.05$) in SigmaPlot 12.

3. Results

3.1. Characterization of CHT NPs and GSNO containing CHT NPs

To obtain NO-releasing chitosan nanoparticles the tripeptide GSH was encapsulated in CHT NPs during the ionic gelation process. This tripeptide, due to the presence of γ -carboxyl groups and amino groups, can interact with the chitosan and resulting in the formation of glutathione-chitosan complex. Through positive electrostatic complexation, using the anionic phosphate groups in TPP and the protonated amine groups in CHT, the formation of CHT NPs as well as S-nitrosoglutathione containing CHT NPs is facilitated (Pelegriño et al., 2017).

FTIR technique was used to investigate the interactions between the different components of nanoparticles. Fig. 1 presents the FTIR spectra of the synthesized CHT NPs, GSNO-CHT NPs, GSNO and GSH. The FTIR spectra of the CHT NPs contains three characteristic peaks at 3434, 1650 and 1320 cm^{-1} . The 3434 cm^{-1} peak is attributed to the stretching vibrations of the amino ($-\text{NH}_2$) and hydroxyl ($-\text{OH}$) groups. The 1650 and

1320 cm^{-1} peaks correspond to C=O and C-H stretching, respectively.

The peaks at 3347 and 3250 cm^{-1} in the FTIR spectra of GSH are the stretching vibrations of imido ($-\text{NH}$) and $-\text{OH}$ functional groups, which are associated with the overlap of the $-\text{NH}$ and $-\text{OH}$ groups. The presence of the peaks at 2525 cm^{-1} indicates the presence of the thiol group in GSH. During the synthesis of GSNO, where sodium nitrite was reacted with GSH molecules, the characteristic thiol ($-\text{SH}$) group in GSH disappears in the spectra of both GSNO and GSNO CHT NPs, which can be attributed to the formation of new nitroso bonds. Additionally, the formation of a new small peak at 1530 cm^{-1} represents the nitroso bond ($\text{N}=\text{O}$) of GSNO (Fig. 1).

It is well known that various experimental factors can influence the size and size distribution of the chitosan nanoparticles during their formation. These factors include the molar mass of chitosan, the chitosan to TPP ratio, the concentration of the aqueous TPP solution, the rate of TPP solution is added dropwise to the chitosan solution (Pelegriño et al., 2017). Each of these variables can substantially impact the resulting NP size and distribution. Fig. 2A presents the particle size distribution of the CHT NPs and GSNO-CHT NPs.

Based on dynamic light scattering studies, using a 3 CHT:1 TPP ratio, the size of the produced CHT NPs was 154.5 ± 3.5 nm. DLS measurements revealed that in the case of GSNO-CHT NPs a higher hydrodynamic size was obtained compared to the initial CHT NPs. The particle size distribution presents two characteristic peaks for GSNO-CHT NPs at 476 ± 64.6 nm and 2540 ± 46.2 nm, suggesting a bimodal distribution. The zeta potential values for the CHT NPs and the GSNO-CHT NPs were found to be $+18.3 \pm 0.6$ mV and $+13.8 \pm 0.5$ mV respectively. The encapsulation efficiency of GSNO within CHT nanoparticles was found to be 89.6 ± 0.35 %. This significant value highlights the electrostatic interactions between GSNO and the nanoparticle components, thereby confirming the successful synthesis of the nanoparticles.

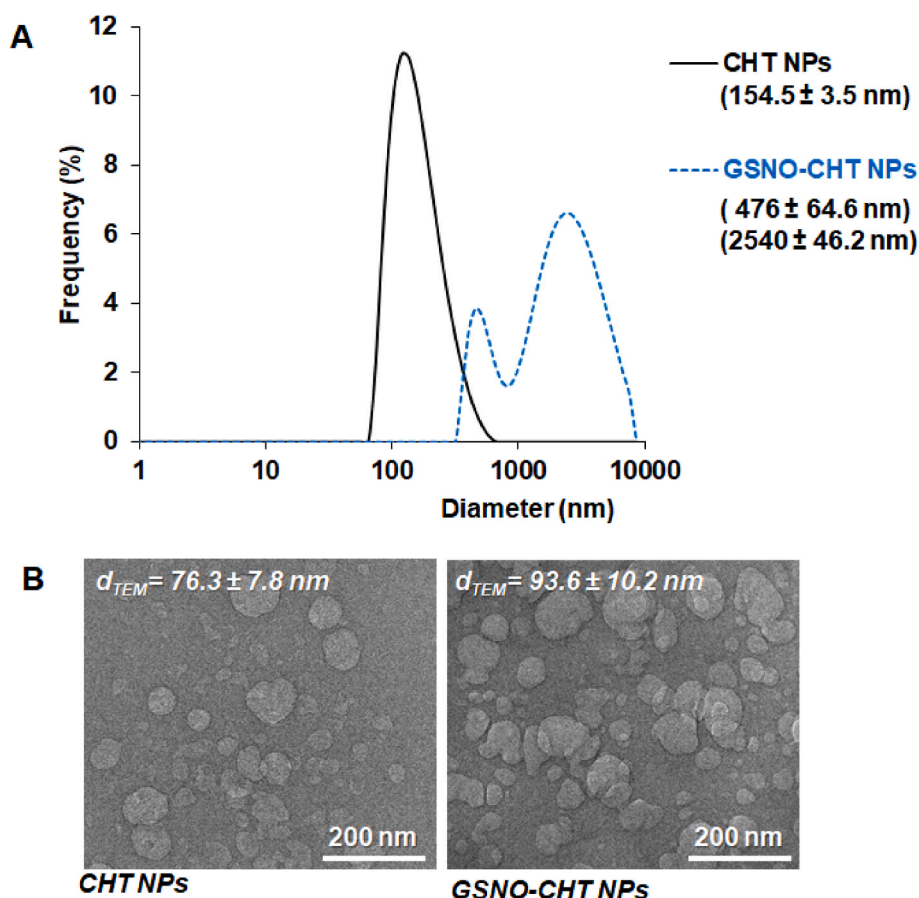


Fig. 2. The particle size distribution of the CHT NPs and GSNO-CHT NPs (A) and representative TEM micrographs of the CHT NPs and GSNO-CHT NPs (B).

Transmission electron microscopy was used to assess the morphology and size distribution of nanoparticles (Fig. 2B). According to representative TEM images of both samples, the nanoparticles showed a spherical morphology. The mean diameter of the CHT NPs was determined to be 76.3 ± 7.8 nm, whereas GSNO-CHT NPs exhibited a significantly larger average diameter of 93.6 ± 10.2 nm. This increase in particle size following GSNO loading confirms successful incorporation of GSNO within the chitosan matrix, leading to structural expansion.

3.2. *In vitro* NO liberation capacity of free and encapsulated GSNO

Using the electrochemical detection method, we followed the kinetics of NO release from the treatment solutions under illumination similar to that applied for plant cultivation (Fig. 3A). The NO concentration of the 250 μ M GSNO solution increased for about 90 min, then remained stable until the 180th min of the measurement and gradually decreased until the end of the measurement. In the case of 500 μ M GSNO concentration, slightly higher NO levels were liberated compared to the lower concentration in the 90th min of the measurement and the NO level remained high after 210 min. The concentration of the released NO reached its maximum between 90 and 120 min in both GSNO doses, which in the case of 250 μ M was ~ 35 nM, while in the case of 500 μ M it was ~ 38 nM. The amount of NO released by 250 μ M GSNO-CHT after 30 min (~ 40 nM) was higher compared to NO levels released by bulk GSNO and started to decrease after 150 min. The concentration of the 500 μ M GSNO-CHT-liberated NO remained stably high between 90 and 210 min and reached a maximum concentration of 54 nM. NO concentrations close to zero nM were measured in both doses of empty CHT suspension in every time point (data not shown).

Both bulk GSNO doses resulted in similar NO concentrations in the solution resulting in a lower NO liberation capacity in the case of the higher donor concentration (Table 1). The NO liberation from 250 μ M GSNO-CHT was 27 % lower than the same concentration of bulk GSNO, but the 500 μ M GSNO-CHT released more NO (by 37 %) than the bulk form, therefore the calculated capacity value slightly increased with the enhancement of the nanodonor concentration (Table 1). The total released NO concentrations and the maximum instantaneous NO concentrations proved to be dependent on the bulk and nanodonor concentration, and the nanoforms showed higher values (Table 1).

Moreover, the NO concentration of the treatment suspensions in the presence of the plant root was monitored every 30 min during the treatment period (120 min, Fig. 3B).

The course of the NO liberation was analogous to that of the *in vitro* measurement, with an initial increase in NO concentration over time, followed by a plateau between 90 and 120 min (Fig. 3B). In the presence of plant roots, the amount of detectable NO was significantly reduced, with values ranging from 4.5 to 6.3 nM at 120 min (Fig. 3B).

Table 1

Nitric oxide-release properties of bulk and nano GSNO (in distilled water, pH 4.6, 24 ± 2 °C).

	[NO donor] (μ M)	released [NO] (nM) after 210 min	NO release capacity (%) ^a	total [NO] released (nM) ^b	max. [NO] (nM) ^c
GSNO	250	33.81	0.013	239.60	34.92
	500	33.87	0.0067	296.07	38.53
GSNO-CHT	250	24.43	0.0097	320.24	50.74
	500	54.36	0.010	378.49	54.36

^a NO release capacity (%) = released NO cc. (210 min) *100/NO donor cc.

^b Total NO released over full duration of the measurement.

^c Maximum instantaneous NO concentration.

3.3. Root cell wall modifications induced by GSNO-CHT and CHT nanoparticles

Since both bulk and CHT-encapsulated GSNOs directly meets the cell wall of the root cells, changes in the cell wall components were also followed in the experiments. Pectin is the component of the cell wall matrix and its level was not notably changed by bulk GSNO, but increased by GSNO-CHT and CHT, which was indicated by the darkening of the ruthenium red staining (Fig. 4A). Qualitative determination of lignin in Brassica root tips suggested that its content was not changed by GSNO, but was increased by CHTs, especially by GSNO-CHT (Fig. 4B). Additionally, detached cells were detected not only in the treated roots but also in the Control samples, indicating that this phenomenon may not be exclusively induced by the treatments and merits further investigation. While the presence of detached cells may suggest border cell release, no specific analysis was performed in this study to confirm this (Fig. 4A and B). Bulk GSNO application likely led to increased callose deposition due to its rapid and possibly excessive NO release, which is known to act as a stress signal and can stimulate callose synthesis as part of a defense response. In contrast, both GSNO-CHT and empty CHT, resulted in decreased callose content, and this effect was concentration-dependent. This reduction might be attributed to the more controlled and sustained release of NO from the nanocapsules, which may modulate the plant's response without triggering strong defense mechanisms like callose deposition. Interestingly, even empty CHT nanocapsules showed a similar effect, suggesting that the chitosan carrier itself may influence callose dynamics, possibly through its interaction with the cell wall or signaling pathways (Fig. 4C and D).

3.4. Rhizosphere acidification as the effect of GSNO-CHT and CHT nanoparticles

Since interactions of roots with exogenous compounds may depend on the pH surrounding the root, putative changes of pH in the immediate

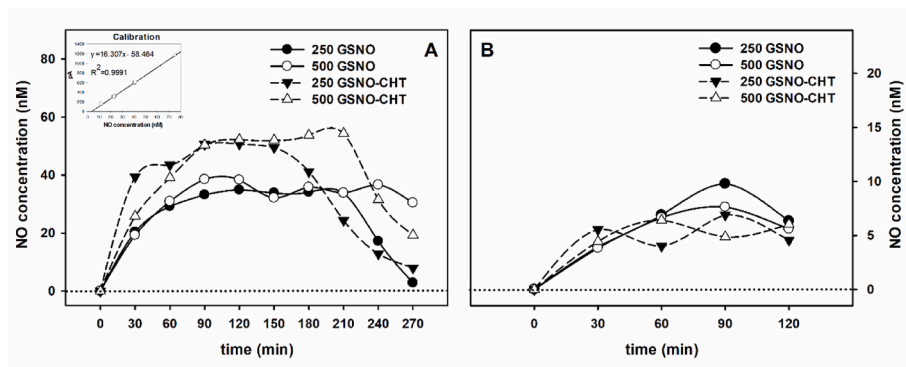


Fig. 3. *In vitro* nitric oxide liberation in treatment solutions. (A) Time course of the NO liberation in 250 and 500 μ M GSNO solution and GSNO-CHT suspensions. Calibration curve with equation and R^2 value is indicated. (B) Time course of the NO liberation in 250 and 500 μ M GSNO solution and GSNO-CHT suspensions in the presence of plant roots.

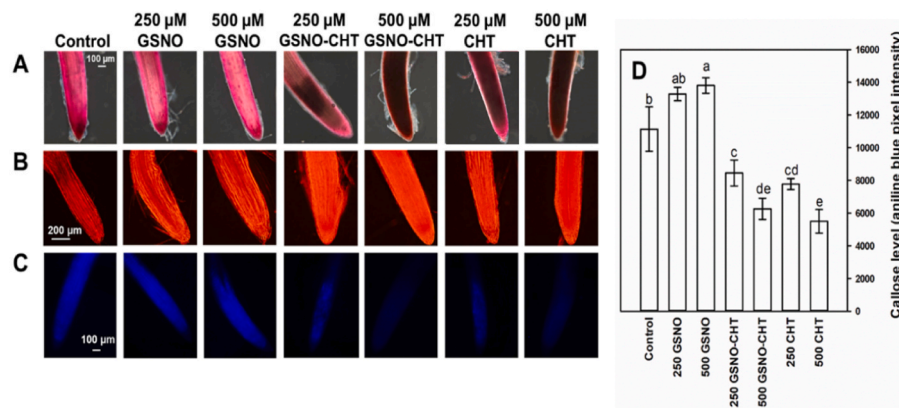


Fig. 4. Changes in cell wall components induced by nanoparticles. Pectin levels indicated by pink colorization of the root tip (ruthenium red staining, **A**), lignin levels indicated by orange colour (phloroglucinol-HCl staining, **B**) and callose levels indicated by blue colour (aniline blue staining, **C**). Scale bars = 100 μm (**A**, **C**) or 200 μm (**B**). Pixel intensity values of aniline blue-associated fluorescence (**D**) in the root tips of *B. napus* treated for 2 h via the root system. Different letters indicate statistically significant differences according to Duncan's test ($n = 10$, $p < 0.05$). (For interpretation of the references to colour in this figure legend, the reader is referred to the Web version of this article.)

vicinity of the root were detected using the bromocresol purple pH indicator. The pH of the GSNO-CHT and CHT treatment suspensions is 4.6, which is why the yellow colour appeared in the culture medium (lower panel of Fig. 5A). Compared to this, significantly higher densities of the yellow bromocresol signal were measured in the presence of the root in the case of the 500 μM GSNO-CHT and 500 μM CHT treatments (Fig. 5A and B). In the case of bulk GSNO, slight rhizosphere acidification (indicated by yellow colour) was detected, but in the case of the 500 μM dose, it was less than the acidification caused by nanoparticles at the same concentration. The acidification proved to be the most intense in GSNO-CHT-treated *B. napus* roots (Fig. 5A and B).

3.5. Internalization of CHT-FITC nanocapsules

The FITC-tagged version of the empty and GSNO-filled CHT nanocapsules were prepared in order to determine whether the nanocapsules internalize *B. napus* root cells during the 2-h treatment period. The successful tagging with FITC was corroborated by the spectrofluorometric determination of the excitation-emission spectrum characteristic for FITC in the nanoparticle suspensions (Fig. S1).

For the microscopic detection, several Controls were used in order to assess the specificity of the observed CHT-FITC signal. No signal was detected in distilled water (DW)-, bulk GSNO-, GSNO-CHT- or CHT-treated samples. In case of free FITC, the detected signal was restricted to the columella cells of the root tip (Fig. S2) indicating that

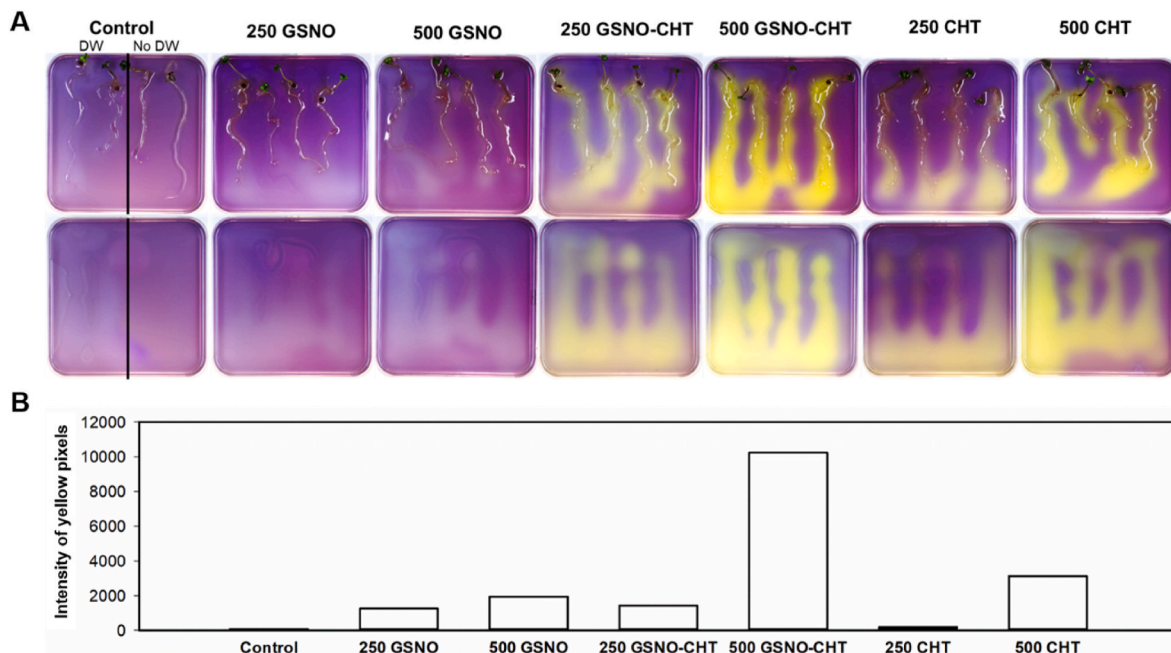


Fig. 5. Rhizosphere acidification induced by nanoparticles. (**A**) Representative photographs taken from Petri dishes with bromocresol purple pH indicator (purple colour at pH 6). The upper row shows pH changes in the presence of both the plants and the treatment suspensions, while the lower row shows pH changes caused by the treatment solutions without plants. Plate widths are 12 cm. (**B**) Densitometric analysis of yellow pixels measured on digital photographs. The values of yellow pixel intensities measured on digital photographs without plants were subtracted from the values of pixel intensities measured on digital photographs with plants. (For interpretation of the references to colour in this figure legend, the reader is referred to the Web version of this article.)

FITC molecules are absorbed by the root cap cells. However, no FITC signal was detected in the root tips of the GSNO-CHT-FITC exposed plants (Fig. S2). In contrast, within the root tip of CHT-FITC-treated seedlings, the cap area showed intracellular FITC signal (Fig. 6A) localized to cytoplasm and/or plasma membrane of the meristem cells (Fig. 6B and C).

3.6. *In planta* NO liberation induced by bulk and nano GSNO

Using uncapsulated GSNO, GSNO-CHT and the empty CHT nanocapsule in elevating concentrations for 2 h via the root system, we found that bulk GSNO did not significantly modify root NO levels, while GSNO-CHT caused a significant increase even at the lowest dose (250 μM), and showed an increase in NO levels dependent on the NP concentration. In the case of the 1000 μM GSNO-CHT treatment, a 2.5-fold endogenous *in planta* NO level was detected compared to the Control (Fig. 7A–D). The presence of CHT nanocapsule alone did not modify the NO level in the root (Fig. 7A–D). In the hypocotyl, NO level elevated with 500 μM bulk GSNO but decreased at 750 and 1000 μM . The CHT-encapsulated NO donor treatment resulted in lower NO levels at 250, 500, and 1000 μM compared to Control, and a similar reduction was caused by the 500 and 1000 μM empty capsules (Fig. 7B–D). In cotyledon cross-sections, NO levels increased only with the 500 μM GSNO-CHT, while bulk GSNO and CHT had no effect (Fig. 7C and D).

These data reflect clear organ-specific differences in NO accumulation. In the hypocotyls and cotyledons (Fig. 7B, C, D), DAF-FM fluorescence remained largely unchanged across treatments and concentrations, indicating limited NO modulation. In contrast, the roots

exhibited a marked, dose-dependent fluorescence increase in response to GSNO-CHT (Fig. 7A–D), likely due to more efficient uptake and sustained NO release by the nanocarrier. Neither bulk GSNO nor CHT alone induced comparable changes, underlining the specific efficacy of the encapsulated formulation in root-targeted NO delivery.

In the case of the 250 μM treatment dose, the NO level of the roots was detected as a function of time, up to 5 h. At 2 h, both the uncapsulated GSNO and the GSNO-CHT caused slight increase in the NO level in the upper region of the primary root, and the evolution of the effect over time was similar in both treatments (Fig. S3 A, C). In the primary root meristem, GSNO-CHT resulted in a moderate NO peak at 2 h, while in the case of CHT the NO level increase was notably lower. It should be noted that after 4 h of treatment, the *in planta* NO level was significantly increasing as the effect of GSNO treatment, but this was lacking in the case of GSNO-CHT (Fig. S3 B, C).

3.7. Bulk and nano GSNO triggers alterations in the expressions of NO-associated genes

To investigate the effects of the treatments on nitric oxide (NO) metabolism in *B. napus*, the expression of key genes involved in NO biosynthesis and signaling was analyzed. *NIA1* and *NIA2* genes encode nitrate reductase, which plays a central role in NO production through the reduction of nitrate to nitrite, and subsequently to NO under certain physiological conditions. *GLB1* and *GLB2* genes encode non-symbiotic hemoglobins, which are implicated in the modulation and scavenging of NO, thereby contributing to NO homeostasis. Among the NO-associated genes in both the root and shoot, the *BnNIA1* gene

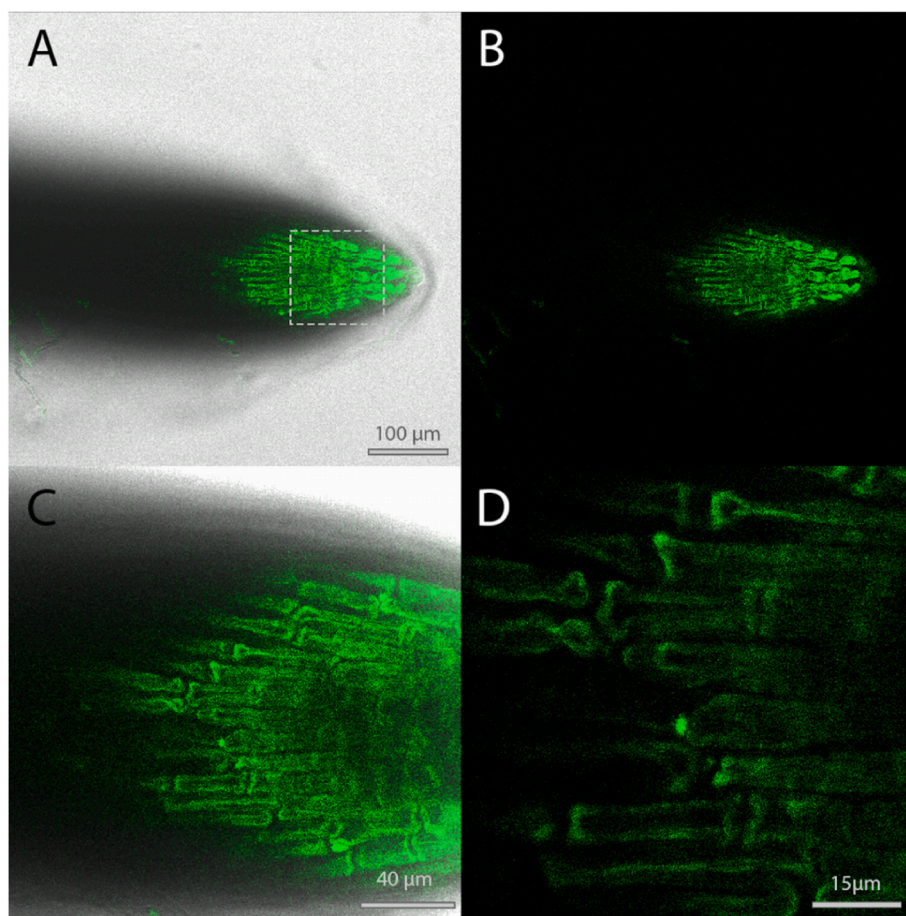


Fig. 6. *In planta* visualization of fluorescently labelled nanoparticles. Representative confocal microscopic images of *B. napus* primary root tips treated with CHT-FITC (500 μM , 2h). Dotted region in (A) represents approximate position of the closeups shown in (C) and (D). Fluorescence and brightfield-overlaid images are shown in panels A and C. Scale bars are 100 μm (A, B), 40 μm (C) and 15 μm (D).

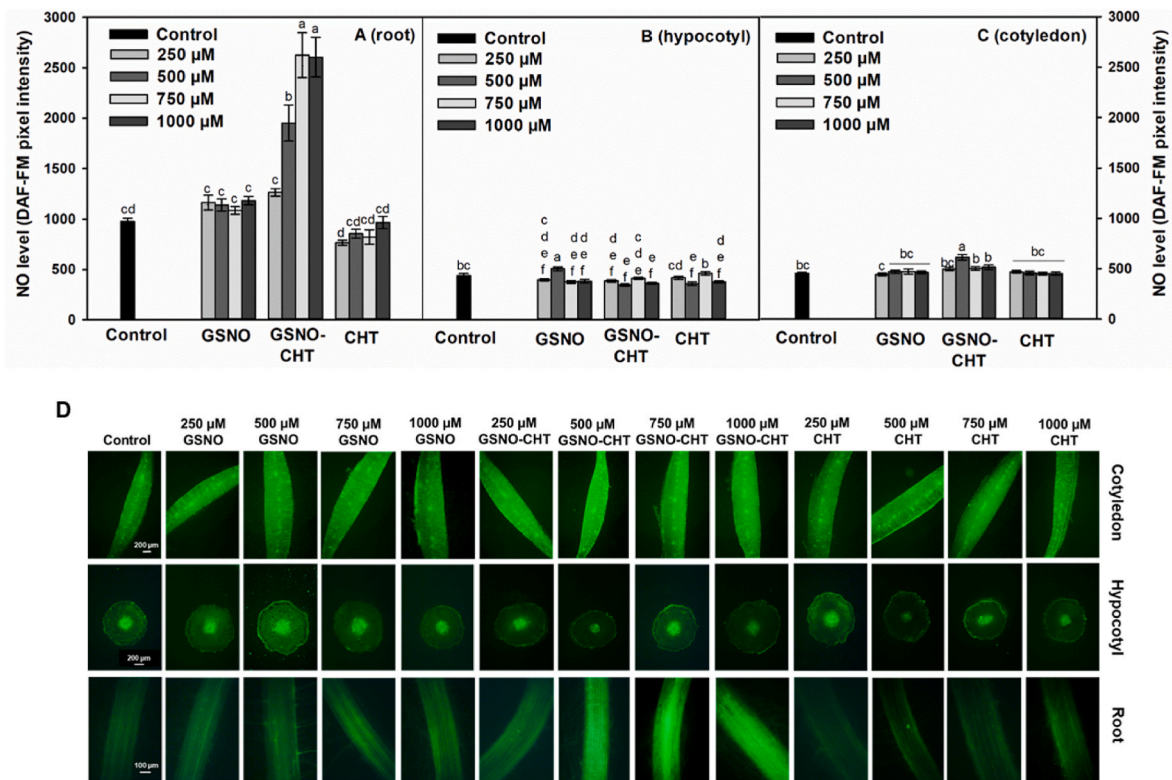


Fig. 7. Nitric oxide levels in organs of *B. napus* seedlings. The seedlings were treated with 0 (Control), 250, 500, 750 or 1000 μ M bulk GSNO, GSNO-CHT or empty CHT for 2 h via the root system. Values of pixel intensities in the root (A), hypocotyl (B) and cotyledon (C). Different letters indicate statistically significant differences according to Duncan's test ($n = 3$, $p < 0.05$). (D) Representative fluorescent microscopic images of DAF-FM DA-labelled roots, hypocotyl cross sections and cotyledon cross sections. Scale bars = 200 μ m (cotyledon and hypocotyl) or 100 μ m (root).

encoding nitrate reductase proved to be strongly GSNO-responsive, as the bulk GSNO increased its expression in a concentration-dependent manner (Fig. 8A and B). Compared to this, the CHT-encapsulated GSNO induced even higher *BnNIA1* expression levels at both doses. As the effect of the 500 μ M GSNO-CHT treatment, *BnNIA1* expression in the root increased 8 times the Control value, and 5 times the Control value in the shoot. CHT nanocapsule did not significantly modify *BnNIA1* expression in the root (Fig. 8A and B). In the shoot, 3-fold induction of *BnNIA1* expression was caused by 250 μ M CHT and a slighter elevation was measured in 500 μ M CHT-treated seedlings (Fig. 8A).

Phytoglobin-encoding *BnGLB1* strongly responded to bulk GSNO treatment in both examined organs (Fig. 8C and D). The 250 μ M GSNO resulted in a 20-fold increase in the expression of *BnGLB1*, and the 500 μ M GSNO caused a 35-fold increase in the root, while the inductions were ~12-fold and 23-fold in the shoot of 250 and 500 μ M GSNO-treated *B. napus*, respectively (Fig. 8C and D). Compared to the free GSNO, GSNO-CHT increased the expression of *BnGLB1* in the roots to a lesser extent, independently from the dosage. The effect of the empty CHT capsule on *BnGLB1* expression was comparable to the level of GSNO-CHT-associated induction in the shoot (Fig. 8C and D). In the case of *BnGLB2*, the trend was similar to the GSNO-induced changes of the *BnGLB1* expression in the root, but the degree of induction was much smaller (2-fold in the case of 500 μ M GSNO, Fig. 8D and E). In the shoot, both 250 and 500 μ M GSNO increased the expression of *BnGLB2*, but not in statistically significant manner. The treatment with GSNO-CHT resulted in slightly diminished *BnGLB2* expression in the root. The CHT capsule at the dosage of 500 μ M significantly reduced the expression of *BnGLB2* in the root and did not affect it in the shoot (Fig. 8E and F).

3.8. Bulk and nano GSNO triggers changes in nitrite levels and GSNO-mediated SNO/GSNO metabolism

Bulk GSNO caused a concentration-dependent but non-significant increase in the nitrite concentration of the seedlings (Fig. 9A). In the case of encapsulated GSNO, the 250 μ M concentration caused a significant increase in the nitrite level, which was further increased by the 500 μ M dose, causing a highly significant nitrite accumulation (Fig. 9A). Regarding SNO, bulk GSNO caused a concentration-dependent increase, which was significant in the case of the 500 μ M dose (Fig. 9B). In the case of GSNO-CHT, the tendency of the SNO content alteration was similar to that of caused by the bulk form, but the 500 μ M treatment resulted in a significantly higher SNO level. The empty CHT capsule did not cause any increase in either nitrite or SNO levels (Fig. 9B).

Beyond measuring total SNO in whole seedlings, we detected GSNO in roots, hypocotyl and cotyledon samples of *B. napus* seedlings using specific antibody labelling (Fig. 10). Interestingly, GSNO levels in the roots were significantly decreased by all treatments compared to Control (Fig. 10A–D). In the case of the bulk GSNO, the decrease of the root's endogenous GSNO level was the most significant, because both doses resulted in an almost 50 % decrease in GSNO-associated fluorescence intensity in the root. In the case of GSNO-CHT NPs, the 250 μ M concentration resulted in a significantly higher GSNO level in the root than in the case of the GSNO treatment, while in the case of the 500 μ M dose, the degree of effect is comparable for bulk and nanoencapsulated GSNO. Additionally, the empty nanocapsule reduced the endogenous GSNO level proportional with the applied dose (Fig. 10A–D). The 2-h root-assisted application of 500 μ M GSNO and 250 μ M GSNO-CHT caused elevation of GSNO level in the hypocotyl, while bulk GSNO and empty CHT at 250 μ M concentration significantly reduced the GSNO level (Fig. 10B). Interestingly, the opposite trend was observed in the GSNO levels of the cotyledon, where 250 μ M bulk GSNO increased and 500 μ M

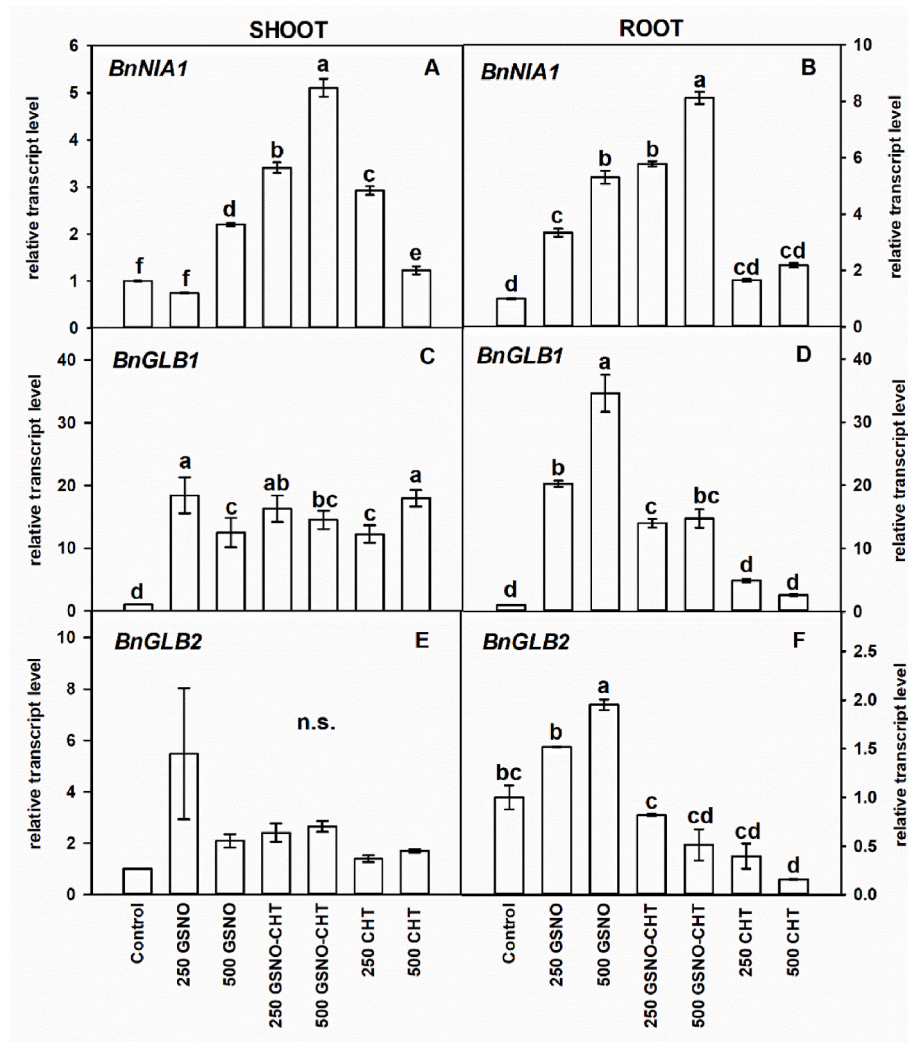


Fig. 8. Changes in the relative transcript levels of NO-associated genes—*BnNIA1* (encoding nitrate reductase), *BnGLB1* and *BnGLB2* (encoding class 1 phytohemoglobins)—in shoots (A, C, E) and roots (B, D, F) of *B. napus* seedlings. The seedlings were treated with 250 or 500 μM bulk GSNO, GSNO-CHT or CHT for 2 h via the root system. Data were normalized using the *B. napus ACTIN7* gene as internal Control. The relative transcript level in Control samples was arbitrarily considered to be 1. Different letters indicate statistically significant differences according to Duncan's test ($n = 3$, $p < 0.05$). n.s. = non-significant.

bulk GSNO decreased the GSNO levels (Fig. 10C).

The most characterized enzyme metabolizing GSNO is GSNOR, and changes in its gene expression and activity can explain the changes of GSNO levels caused by nano and non-nano NO donor treatments.

In the shoot, the expression of *BnGSNOR1* decreased as the effect of GSNO and GSNO-CHT dosages, but the diminution proved to be more significant in shoots of 250 μM exposed plants compared to the higher concentration (Fig. 11A). The presence of the CHT nanocapsule exerted slight effect on *BnGSNOR1* expression of the shoot (Fig. 11A). In the root, GSNOR expression did not change significantly neither in response to uncapsulated GSNO, nor in the case of GSNO-CHTs, but decreased in response to CHT treatment (Fig. 11B).

The bulk GSNO caused a concentration-dependent increase in GSNOR activity measured in whole seedlings (Fig. 11C). In the case of GSNO-CHT, the effect was similar, but the increase of GSNOR activity was much smaller and not statistically significant. Moreover, CHT supplementation did not alter GSNOR activity compared to Control (Fig. 11C).

3.9. Bulk and nano GSNO alter the levels of cys and cys-containing metabolites

The precursors of GSH are cysteine and gamma-glutamylcysteine (gEC). The amounts of these together with GSH were measured, and the effect of nano and bulk GSNO was compared (Fig. 12).

The reduced form of free Cys exhibited a notable increase in concentration as a function of GSNO dosages, which resulted in a corresponding elevation in total Cys. The amount of Cys_{ox} decreased compared to the Control as a result of both GSNO doses. The effect of 250 μM GSNO-CHT is comparable to that of free GSNO, with an elevation in Cys_{red} and a diminution in Cys_{ox} . Treatment with 500 μM GSNO-CHT resulted in a significant reduction in the amount of Cys_{ox} , but did not significantly alter the content of Cys_{red} . Interestingly, in the presence of the 500 μM empty CHT capsule, the amount of reduced and oxidized Cys was at the Control level, while in the case of 250 μM CHT, the amount of Cys_{ox} increased (Fig. 12A).

The gEC is the direct precursor of GSH and its formation is the rate-limiting step of the synthesis. Neither bulk GSNO nor nano GSNO resulted in an increase in gEC content (Fig. 12C). Both doses of the empty CHT capsule resulted in a slight increase in gEC amounts (Fig. 12B), with no change in total Cys levels (Fig. 12A), and did not lead

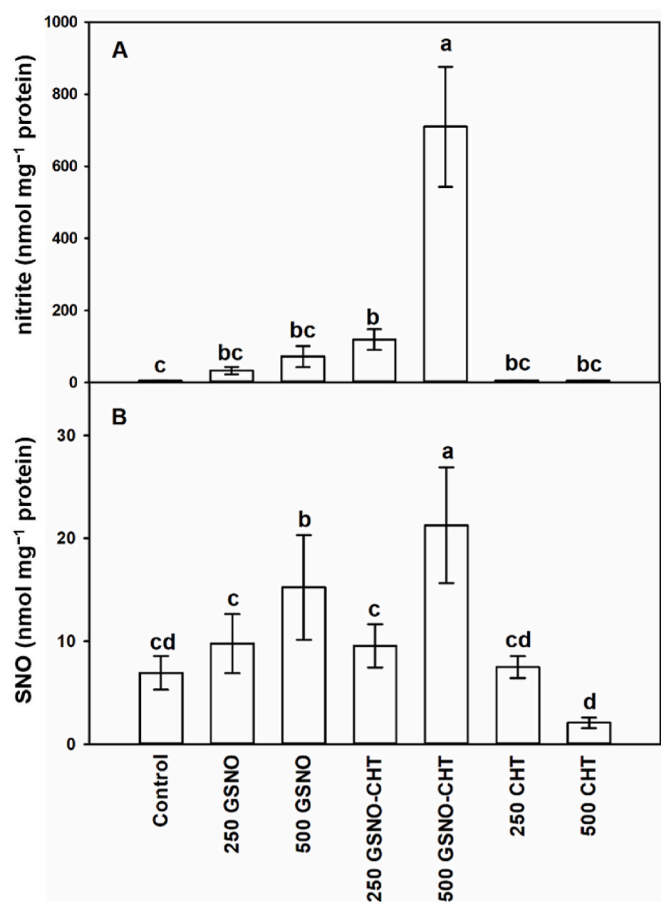


Fig. 9. Nitrite (A) and S-nitrosothiol (B) concentrations in *B. napus* seedlings. The seedlings were treated with 250 or 500 μM bulk GSNO, GSNO-CHT or CHT for 2 h via the root system. Different letters indicate statistically significant differences according to Duncan's test ($n = 3$, $p < 0.05$).

to elevated GSH amounts in comparison to the Control (Fig. 12C). The only treatment which resulted in significantly higher GSH levels compared to Control was the 250 μM bulk GSNO (Fig. 12C).

3.10. Bulk and nano GSNO differentially modify ROS levels and tyrosine nitration

The 500 μM GSNO supplementation significantly increased ONOO⁻ level in the root, while GSNO-CHT and CHT did not significantly modify it compared to the Control (Fig. 13A–G). In the hypocotyl, the lower concentration of GSNO-CHT as well as both concentrations of CHT led to a slight but statistically significant reduction in ONOO⁻ levels (Fig. 13B). However, none of the treatments altered ONOO⁻ levels in the cotyledon (Fig. 13C). Hydrogen peroxide level of the root was slightly decreased by the lower concentration of the bulk GSNO, and was not significantly altered by 500 μM GSNO. The GSNO-CHT treatments resulted in an almost 70 % decrease in H₂O₂ levels, while both concentrations of CHT resulted in 80–85 % reduction of root H₂O₂ levels (Fig. 13D–G). In the hypocotyl, the tendency of H₂O₂ level changes was similar to that of the root, since both dosages of GSNO-CHT and CHT caused a significant reduction (Fig. 13E). Interestingly, the superoxide radical level was not changed by the addition of GSNO in the root, but was increased both by nanoencapsulated GSNO and the empty CHT capsule in a dose-dependent manner (Fig. 13F and G). The amount of 3-nitrotyrosine was significantly increased by both doses GSNO, which is indicated by the intensification of the immunopositive signal in several protein bands (indicated by arrows on Fig. 13H and Fig. S4). In the case

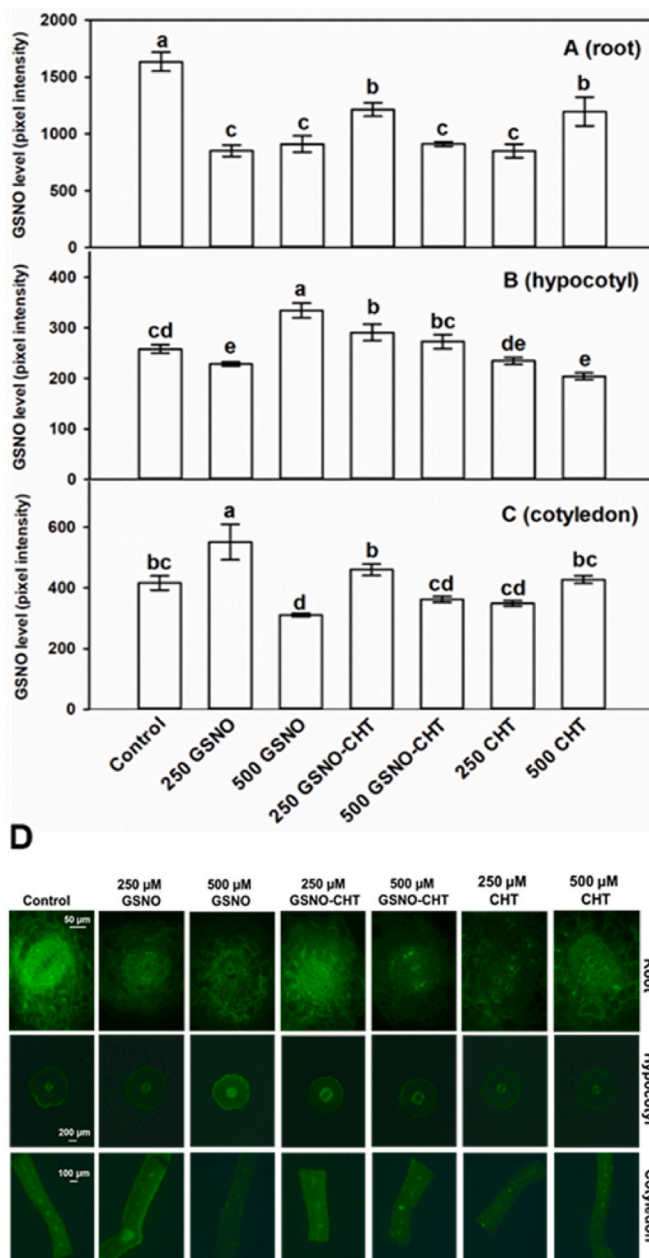


Fig. 10. S-nitrosothione levels in the root (A), hypocotyl (B) and cotyledon (C) of *B. napus* seedlings. The seedlings were treated with 250 or 500 μM bulk GSNO, GSNO-CHT or CHT for 2 h via the root system. Different letters indicate statistically significant differences according to Duncan's test ($n = 3$, $p < 0.05$). (D) Representative fluorescent microscopic images showing cross sections of Brassica cotyledons, hypocotyls and roots labelled with FITC-tagged secondary antibody against anti-GSNO primary antibody (see details in Materials and methods). Scale bar = 50 μm .

of GSNO-CHT, significant change was not observed in the degree of tyrosine nitration compared to the Control. CHT nanocapsule exposure resulted in a small decrease in the level of tyrosine nitration or did not change its extent (Fig. 13H and Fig. S4).

4. Discussion

4.1. Movement and utilisation of GSNO is modified by CHT encapsulation

The data obtained during the detailed evaluation of the synthesized NPs are in accordance with those described by others for similar NPs (Xu

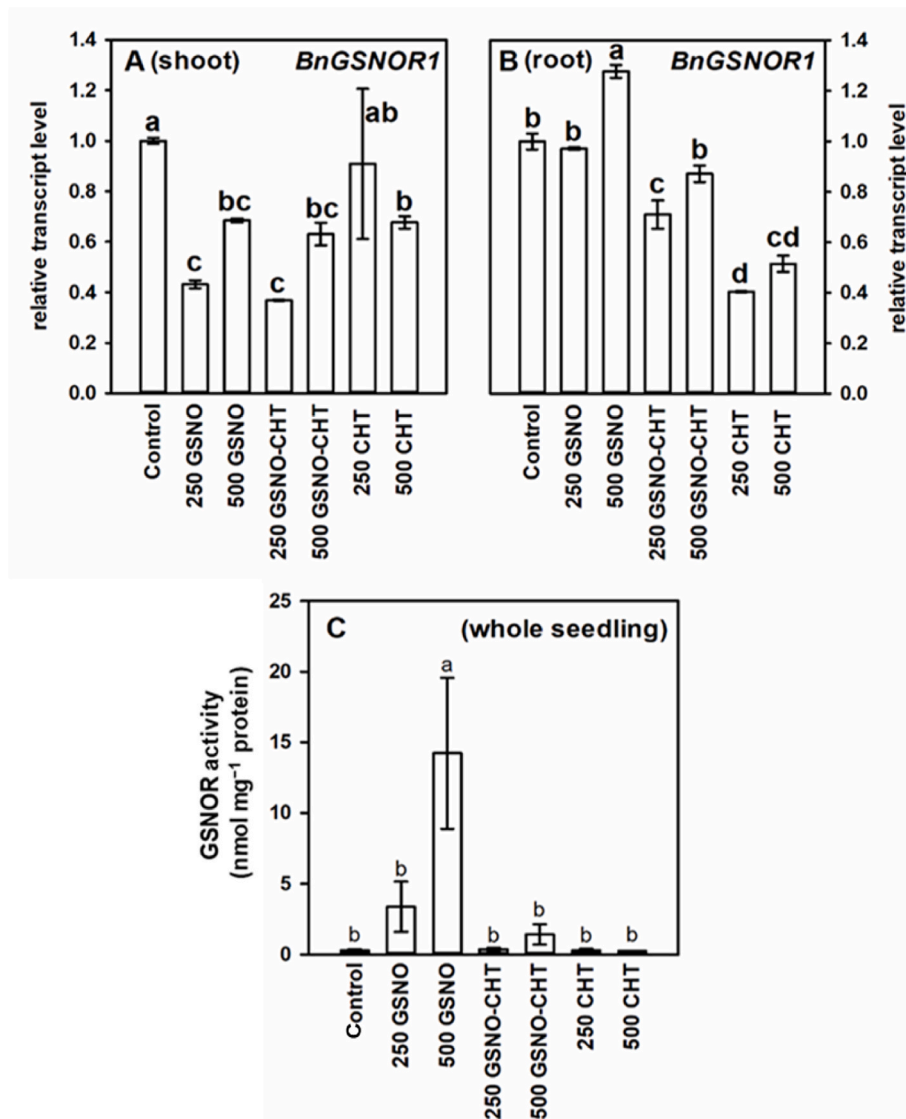


Fig. 11. Gene expression (A, B) and activity (C) of GSNOR in *B. napus*. The seedlings were treated with 250 or 500 μM bulk GSNO, GSNO-CHT or CHT for 2 h via the root system. Relative transcript level of *BnGSNOR1* in the shoot (A), and root (B) of *B. napus* seedlings. Data were normalized using the *B. napus ACTIN7* gene as internal Control. The relative transcript level in Control samples was arbitrarily considered to be 1. (C) Activity of GSNOR in whole seedlings of *B. napus*. Different letters indicate statistically significant differences according to Duncan's test ($n = 3, p < 0.05$).

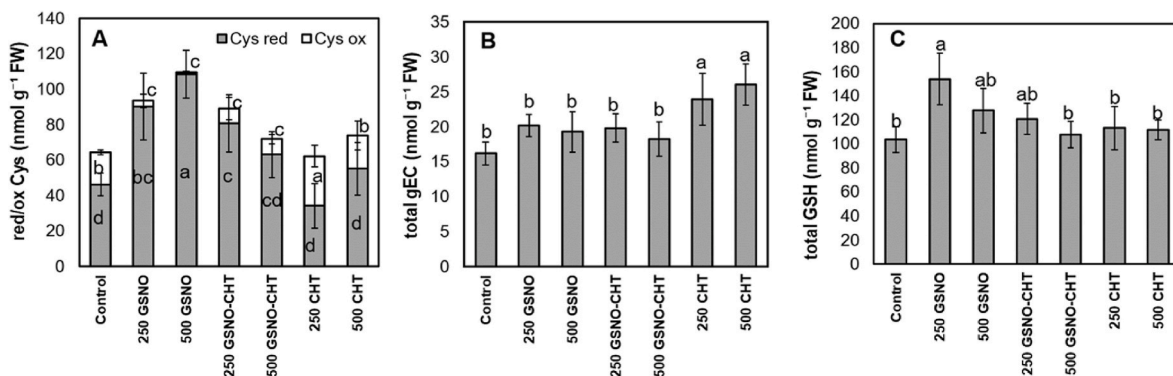


Fig. 12. Concentration of cysteine (Cys) and Cys-containing metabolites in *B. napus* seedlings. The seedlings were treated with 250 or 500 μM bulk GSNO, GSNO-CHT or CHT for 2 h via the root system. Concentration of reduced and oxidized Cys (A), total amount of gamma-glutamylcysteine (gEC, B) and reduced glutathione (GSH, C). Different letters indicate statistically significant differences according to Duncan's test ($n = 3, p < 0.05$).

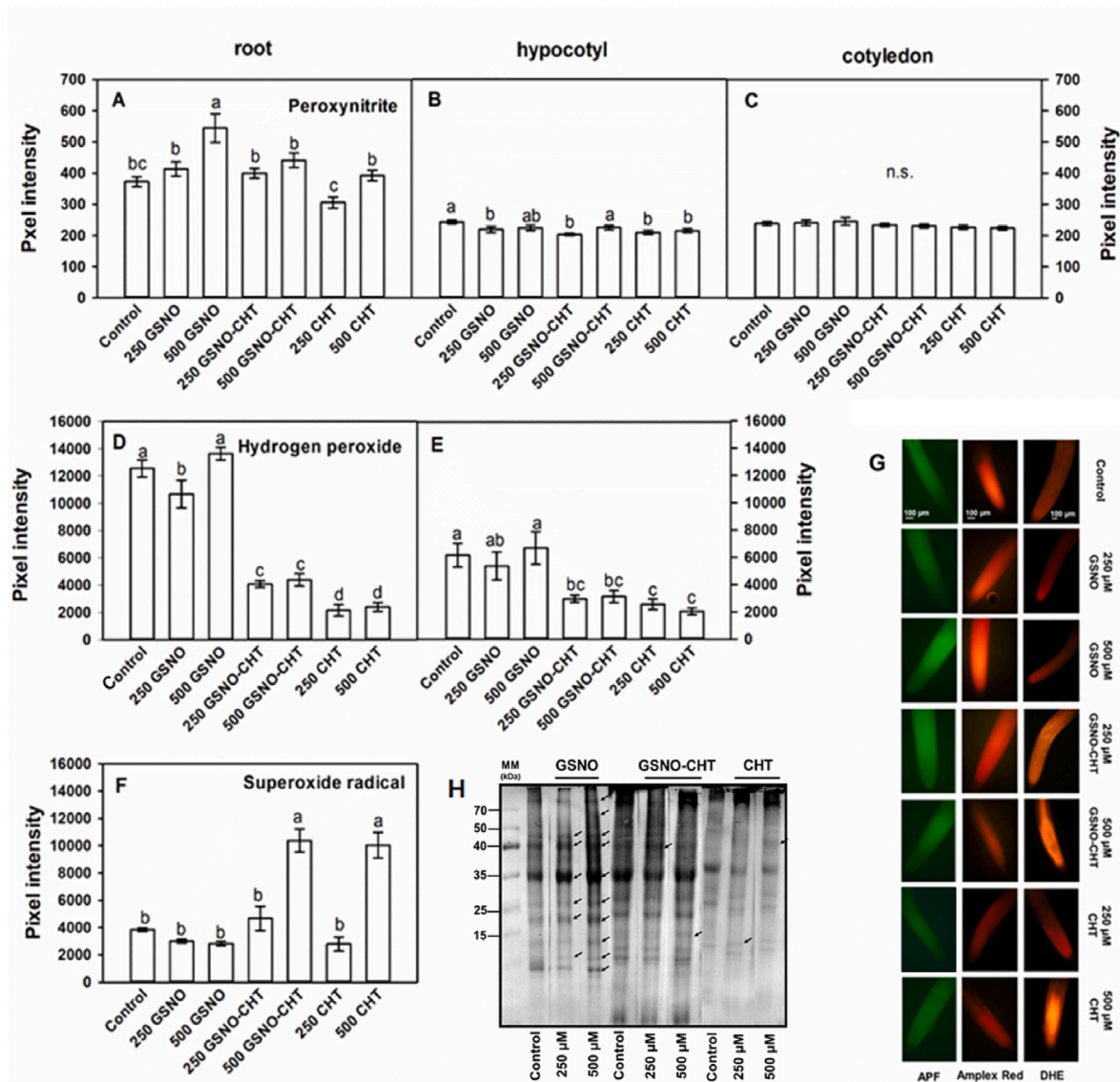


Fig. 13. Level of reactive species and tyrosine nitration in the organs of *B. napus* seedlings. The seedlings were treated with 250 or 500 μM bulk GSNO, GSNO-CHT or CHT for 2 h via the root system. Values of pixel intensities associated with peroxynitrite (A, root; B, hypocotyl; C, cotyledon), hydrogen peroxide (D, root; E, hypocotyl) and superoxide radical (F, root). Different letters indicate statistically significant differences according to Duncan's test ($n = 10$, $p < 0.05$). (G) Representative fluorescent microscopic images of *B. napus* root tips labelled with different fluorophores to detect peroxynitrite (APF), hydrogen peroxide (Amplex Red) and superoxide radical (DHE). (H) Representative Western blot showing 3-nitrotyrosine abundance in whole Brassica seedlings. MM = molecule marker. Treatment-associated increase of the signal is indicated by arrows. (For interpretation of the references to colour in this figure legend, the reader is referred to the Web version of this article.)

and Du, 2003; Pelegrino et al., 2017, 2018; Shah et al., 2017; Popova et al., 2020). Encapsulation enhances the stability and controlled release of NO donors, as shown in previous studies (e.g., Pereira et al., 2015; Ma et al., 2019). Consistent with this, GSNO-CHT exhibits a more sustained NO release, especially at higher concentrations, compared to bulk GSNO. This aligns with Silveira et al. (2019), who found that chitosan matrices facilitate extended NO release. The outcomes indicate that GSNO-CHT maintains higher release capacity and peak NO levels at higher doses, while bulk GSNO displayed concentration-independent release. Additionally, the negligible NO release from empty chitosan capsules confirms that NO release is solely from GSNO. Additionally, the NO release kinetics in the presence of plant roots suggest that a considerable part of the released NO is diffused into root tissues (Fig. 3).

NPs can enter root cell walls through pores, which they can modify, potentially altering the wall's composition (reviewed by Kurczyńska et al., 2021). Pectin is the component of the cell wall matrix and its level

was not significantly changed by free GSNO, but increased by GSNO-CHT and CHT (Fig. 4). Similar to this, nY_2O_3 NPs resulted in up to 58 % increase in pectin (Chen et al., 2021). In a more detailed study, methylesterified homogalacturonan (a major pectic component of the cell wall) was observed in rhizodermal walls in AuNP-treated barley roots but was not detected in Control roots (Milewska-Hendel et al., 2021). Callose is known to play a role in plant response to pathogens, heavy metals or mechanical damage (Li et al., 2023), which means that the applied concentration and duration of the bulk GSNO treatment is perceived as a stress for the plant. Supporting our results, NO-induced callose deposition has been evidenced *inter alia* in virus-infected soybean (Xiao et al., 2018) and in tomato infected by fungal pathogen (Noorbakhsh and Taheri, 2016). At the same time, CHT is known to induce callose deposition as a part of the plant defence mechanisms (Sravani et al., 2023; Bertrand et al., 2024; Suwanchaikasem et al., 2024). In this experimental system, CHT nanocapsules did not cause

callose increase which might be attributed to the more controlled and sustained release of NO from the nanocapsules, which may modulate the plant's response without triggering strong defense mechanisms like callose deposition. However, the nanocapsules not only failed to increase callose level but decreased it (Fig. 4), which needs further evaluation. We suspect that the effect of CHT NPs on callose levels may differ in plant species (Kacziba et al., 2023), and may also depend on the presence or the absence of a stressor. Although, CHT-associated lignification observed in our short-term (2h) experiments (Fig. 4) are supported by data in other experimental systems (e.g., Sravani et al., 2023; Suwanchaikasem et al., 2024; Bertrand et al., 2024). The peeling layers or mucilage observed in root images (Fig. 4A and B) likely result from changes in cell wall components induced by GSNO and chitosan treatments. Ruthenium red staining showed increased pectin levels with GSNO-CHT and CHT, while lignin content also rose notably in these treatments. These cell wall modifications may contribute to border cell release or mucilage formation. However, specific analysis of border cell release was beyond the scope of this study (Fig. 4). The specific analysis of border cell release or mucilage formation is a subject of a future study. Our study highlights that CHT-encapsulated NPs can strengthen cell wall integrity via the complex and rapid interactions with plant root cell walls.

Moreover, we showed that GSNO-CHT and CHT significantly acidified the rhizosphere, with the strongest effect observed at higher concentrations (Fig. 5). This acidification, likely due to organic acid exudation by roots (e.g., malate, citrate, fumaric acid), was more pronounced than with bulk GSNO treatments, suggesting that mainly the CHT NPs are responsible for modifying root exudation processes (Suarez-Fernandez et al., 2020). These findings are supported by the research of Sun et al. (2023), who demonstrated that NP absorption and transformation by roots involve complex interactions with root exudates and architecture.

Our results suggest that within 2 h, GSNO-CHT-FITC doesn't enter the root cells, while the empty CHT-FITC nanocapsule interacts with the wall or membrane of the root meristem cells without penetrating those (Fig. 6). The few results on the *in planta* presence of CHT-FITC NPs indicate that those have the potential to internalize into seeds, leaves and roots of different species (e.g., tea plant, wheat, tobacco) during several days of exposure (1–6 days) (Chandra et al., 2015; Li et al., 2019; Scarpin et al., 2023; Sousa et al., 2024). The smaller size of empty CHT nanocapsule compared to the GSNO-CHT (Fig. 2) may result in its enhanced internalization capacity. Furthermore, compared to CHT, GSNO-CHT induced more intense rhizosphere acidification (Fig. 5), which might lead to the disintegration of the NPs and consequently the absence of FITC signal in the root cells.

In the root, the concentration dependence of the GSNO-CHT-induced NO level increase suggests that the presence of NP directly causes the enhancement of the NO levels. However, the possibility that NPs alter cellular uptake of DAF-FM DA probe has not been directly studied, the similar fluorescence levels in control and CHT-treated root as well as the lack of DAF-fluorescence induction due to CHT treatment let us assume that NPs don't significantly influence the uptake of DAF-FM DA dye. The encapsulation of GSNO in CHT NPs significantly enhances its NO delivery efficiency, with GSNO-CHT releasing more NO than free GSNO during the 4-h period. The presence of elevating dosages of CHT nanocapsule did not cause a significant increase in the root NO level confirming that the NO level induction is GSNO-associated and not related to the CHT capsule itself (Fig. 7). In the hypocotyl, NO-associated fluorescence signal is intense in the central cylinder suggesting the presence of NO in the vascular tissue (reviewed by Kolbert et al., 2024). The short-term bulk NO donor treatment caused minor changes in hypocotyl NO levels, and the higher treatment concentration in the case of GSNO-CHT NP caused a change in cotyledons' NO level, which suggests a rapidly operating NO-associated signalling in the seedlings. Both GSNO and GSNO-CHT caused an increase in *in planta* NO levels after 2 h, but the effects of the different GSNO forms are tissue-specific, with

GSNO-CHT having a stronger impact in the primary root meristem. This result might draw attention to the importance of the spatial distribution of NO-related signals (Fig. 7).

4.2. Bulk and nano GSNO may trigger different metabolite changes in plants

Nitrate reductase has been proven to participate in NO synthesis particularly in the root (Rockel et al., 2002), and its expression has been shown to respond to exogenous NO treatment (Antoniu et al., 2013). Following the 2-h-long incubation, GSNO and GSNO-CHT strongly induced *BnNIA1* gene expression with GSNO-CHT showing a higher induction, while the unchanged expression as the effect of CHT suggest GSNO-responsiveness of *BnNIA1* expression in the root (Fig. 8). The lower rates of *BnNIA1* and *BnGLB1* induction and the modifying effect of empty CHT in the shoot system compared to the root implies that in contrast to the direct, primer NO effect in the root, the shoot might be exposed to secondary, non NO-specific effects of the treatments. The bulk GSNO exhibits organ-specific effect on *BnGLB2* expression, enhancing its transcript level in root but not affecting it in shoots. Furthermore, this gene proved to respond only to bulk GSNO but not to GSNO-CHT. In the case of 500 μ M-exposed roots, it is fulfilled that *BnNIA1* and *BnGLB1* are early GSNO-responsive genes and the rate of their induction might be associated with the NO accumulation caused by the treatments. It has to be noted that the GSNO/GSNO-CHT-triggered gene inductions show organ- and concentration dependence. Additionally, the GSNO/GSNO-CHT induced gene expressions do not show a direct correlation with NO levels in *B. napus* organs, which raises the possibility that the genes do not regulate NO homeostasis but have other functions in this system.

Beyond participating in NO metabolism, NR is one of the key enzymes in nitrate metabolism, since it catalyses the reduction of nitrate to nitrite (Campbell, 1999). The changes in seedlings' nitrite concentration are similar to the alterations in *BnNIA1* gene expressions measured in roots and shoots (Fig. 9), which suggests that GSNO-CHT may cause nitrite accumulation in seedlings partly by inducing NR at the gene level. The concentration-dependent nitrite accumulation indicates a direct GSNO effect, and the ineffectiveness of CHT supports GSNO specificity of the effect. Moreover, higher rate of nitrite accumulation was caused by 500 μ M GSNO-CHT compared to the same concentration of the bulk GSNO which may contribute to the greater NO formation (Fig. 9) via non-enzymatic reduction reactions (Wang and Hargrove, 2013). Similar to these, both GSNO forms elevated SNO levels, with GSNO-CHT inducing a higher accumulation at 500 μ M. The empty CHT capsule had no observable impact on SNO levels reflecting the GSNO-specificity of the observed effect. The concentration-dependence of GSNO-triggered SNO accumulation suggests a rapidly activating SNO-associated NO signalling in the seedlings. These results are supported by elevated SNO levels measured in S-nitroso-mercaptosuccinic acid-chitosan (SN-MSA-CNP)-treated *Zea mays* (Oliveira et al., 2016), *Heliocarpus popayanensis*, *Cariniana estrellensis* (Lopes-Oliveira et al., 2019; do Carmo et al., 2021), and GSNO-CNP, S-nitroso-N-acetylcysteine-chitosan (SNAC-CNP) or SN-MSA-CNP-treated sugarcane (Silveira et al., 2021). Among the SNOs, the highly stable GSNO is a widely accepted storage and transport form for the NO signal (Hogg, 2002; Martínez-Ruiz and Lamas, 2007). The detection of its content at tissue-level can give an idea of the fast root-shoot communication due to the NO donor/nanodonor application via the root.

The endogenous GSNO levels were reduced locally in the root in a non-GSNO-specific manner (Fig. 10). At certain concentrations of bulk and encapsulated GSNO in the hypocotyl, GSNO levels increased, which suggests a certain degree of root-shoot translocation. Collectively, the levels of endogenous GSNO do not show concentration- or organ-dependence, which can be explained by the complex processes that influence the current *in planta* GSNO level. The expression of *BnGSNOR1* in both organs is reduced by GSNO-CHT, while bulk GSNO affects it in an

organ-dependent manner. Similarly, empty CHT also diminished *BnGSNOR1* expression, suggesting that the effect of GSNO-CHT is due to the effect of the CHT capsule (Fig. 11). Similar to our results, *GmGSNOR1* expression was significantly decreased by the application of chitosan or chitosan-encapsulated GSNO nanoparticles in soybean (Methela et al., 2023b). The activity of GSNOR shows a GSNO-specific induction with a much more significant effect in the case of the bulk GSNO compared to GSNO-CHT (Fig. 11). The GSNO-induced GSNOR activation is inversely proportional to the amount of NO released by the donor suggesting the direct involvement of GSNOR in regulating SNO/GSNO levels. The changes in gene expression do not correlate with the induction of the enzyme activity and one possible mechanism for regulation is the PTM of GSNOR activity by bulk GSNO. The GSNOR activity is known to be regulated by redox-based PTMs. The PTM directly associated with NO is S-nitrosation, the GSNO-triggered increase of which was indicated by the elevation of SNO levels (Fig. 9). However, S-nitrosation of Cys has been shown to inhibit GSNOR activity (Tichá et al., 2017; Zhan et al., 2018). Additionally, H₂O₂-catalysed activity loss of GSNOR has also been evidenced (Kovacs et al., 2016). According to the results of Matamoros et al. (2020) with *Lotus japonicus* GSNORs, glutathionylation also inhibits the enzyme activity, while reducing conditions and hydrogen sulphide-mediated cysteine persulfidation activates LjGSNORs. These are conceivable secondary effects of GSNO supplementation, but further studies are needed to identify the possible PTM(s) modulating *BnGSNOR* in this system.

In the presence of GSNO, the system undergoes a shift towards Cys_{red}, with an increase in total Cys (Fig. 12). The elevation in the levels of free Cys is toxic above a threshold concentration and may result in loss of sulphur, therefore free Cys accumulation is thought to be an indicator of stress condition (Zagorchev et al., 2013). Free Cys accumulation is significant in the case of bulk GSNO and less pronounced in the case of encapsulated GSNO suggesting that particularly bulk GSNO causes stress in the seedlings. The lower dosage of empty CHT capsule induces Cys oxidation without influencing the total amount of Cys. Neither bulk GSNO nor nano GSNO results in an increase in gEC content. This suggests that the increase in Cys does not result in an increase in gEC and thus GSH synthesis. The only treatment which resulted in significantly higher GSH levels compared to Control was the 250 μM bulk GSNO (Fig. 12). Since this is not related to changes in the amount of precursors, we hypothesize that GSNO might not increase GSH levels by modifying its biosynthesis, but rather affects its degradation.

4.3. Bulk and nano GSNO differentially modify ROS levels and tyrosine nitration

The superoxide radical levels in the roots were unaffected by bulk GSNO but increased in a dose-dependent manner with both GSNO-CHT and the empty CHT capsule (Fig. 13), indicating that the CHT capsule has a dominant effect on superoxide generation. Similar to this, the observed H₂O₂ level diminution in the root and hypocotyl is mainly associated with the presence of CHT capsule. These indicate that the presence of CHT capsule causes disturbance in ROS homeostasis mainly in the root system directly contacting the nanomaterials. It is in contrast to the numerous publications in which CHT in its bulk or nano form exerts antioxidative effects in abiotic and biotic stressed plant species (Ji et al., 2022), and draws attention to the possible oxidative stress inducing effect of CHT NPs even in short-term applications. Interestingly, peroxynitrite levels do not respond to NPs, but are elevated by the bulk GSNO and these alterations are dominant in the root with slightly affected or unaffected ONOO⁻ levels in aerial plant parts (Fig. 13). The bulk GSNO-triggered ONOO⁻ increase might be associated with the intensified tyrosine nitration which mainly results in activity loss and degradation of the target proteins and is considered to be the main marker of nitrosative stress (Kolbert et al., 2017; Corpas et al., 2021). GSNO-CHT had no significant effect either on the ONOO⁻ levels or the physiological nitration state of the proteome suggesting that the

CHT-encapsulated form of GSNO doesn't cause nitrosative stress in the seedling.

Overall, our results suggest that delivering NO through GSNO-CHT NP is a more efficient and balanced way to influence plant physiology than using bulk GSNO. The gradual and controlled NO release from GSNO-CHT seems to support more fine-tuned responses at the molecular level, such as stronger gene expression and more stable SNO accumulation, without triggering stress-related side effects like those seen with bulk GSNO. At the same time, GSNO-CHT helps manage ROS levels in a more regulated way, supporting redox homeostasis rather than disturbing it. These combined effects lead to a more favorable metabolic profile, indicating that GSNO-CHT can enhance the plant's internal signaling and defense systems without overwhelming them. This highlights the potential of GSNO-CHT as a more refined tool for modulating NO signaling and redox balance in plants.

5. Conclusion

The present study applied a model system in which *B. napus* seedlings were exposed to a short term bulk GSNO, chitosan-encapsulated GSNO NPs or empty chitosan NPs treatments via their root system. The results reveal the advantages of GSNO-CHT NPs over bulk GSNO. Nano encapsulation of GSNO results in more intense and slightly more sustained NO liberation *in vitro* compared to the conventional GSNO form. Moreover, NO accumulation and induction of SNO signalling by encapsulated GSNO is greater than by bulk GSNO. The results suggest that the NO/SNO induction of GSNO-CHT is GSNO-specific. Bulk GSNO-triggered accumulation of free cysteine suggests stress-state of the seedlings in contrast to the milder effect of GSNO-CHT. Encapsulation of GSNO prevents nitrosative stress induction. Additionally, GSNO-CHT internalization in plant roots is much less efficient compared to the empty CHT nanocapsule. However, more efforts are needed to clarify additional molecular details of GSNO-CHT effects, these results demonstrate the efficacy of GSNO-CHT as an effective, controlled NO donor for plants.

CRediT authorship contribution statement

Dóra Kondak: Writing – review & editing, Writing – original draft, Visualization, Investigation. **Ágota Deák:** Writing – review & editing, Writing – original draft, Investigation. **Andrea Rónavári:** Writing – review & editing, Investigation. **Tamás Bodor:** Investigation. **Selahattin Kondak:** Investigation. **Oluwatosin Peace Adedokun:** Investigation. **Péter Benkő:** Writing – original draft, Investigation. **Réka Szöllősi:** Investigation. **Gabriella Szalai:** Investigation. **Tibor Janda:** Writing – review & editing, Supervision. **Ferhan Ayaydin:** Writing – review & editing, Writing – original draft, Investigation. **Christian Lindermayr:** Writing – review & editing, Writing – original draft, Supervision. **Zoltán Kónya:** Writing – review & editing. **Zsuzsanna Kolbert:** Writing – review & editing, Writing – original draft, Visualization, Supervision, Funding acquisition, Conceptualization.

Funding

This work was supported by the National Research, Development and Innovation Office of Hungary under grant No. K 135303 (Zs.K.) and by the “Lendület” MOMENTUM Project of the Hungarian Academy of Sciences (LP2023-14/2023). The manuscript is prepared with the professional support of the University Research Scholarship Program of the Ministry of Culture and Innovation, Financed from the National Research, Development and Innovation Fund (EKÖP-24-3-SZTE-521). F. A was supported by EU's Horizon 2020 Research and Innovation Program (SGA No. 739593).

Declaration of competing interest

The authors declare that they have no known competing financial interests or personal relationships that could have appeared to influence the work reported in this paper.

Appendix A. Supplementary data

Supplementary data to this article can be found online at <https://doi.org/10.1016/j.plaphy.2025.110184>.

Data availability

Data will be made available on request.

References

- Antoniou, C., Filippou, P., Mylona, P., Fasoula, D., Ioannides, I., Polidoros, A., Fotopoulos, V., 2013. Developmental stage- and concentration-specific sodium nitroprusside application results in nitrate reductase regulation and the modification of nitrate metabolism in leaves of *Medicago truncatula* plants. *Plant Signal. Behav.* 8 (9), e25479. <https://doi.org/10.4161/psb.25479>.
- Barroso, J.B., Corpas, F.J., Carreras, A., Rodríguez-Serrano, M., Esteban, F.J., Fernández-Ocaña, A., del Río, L.A., 2006. Localization of S-nitrosoglutathione and expression of S-nitrosoglutathione reductase in pea plants under cadmium stress. *JXB* 57 (8), 1785–1793. <https://doi.org/10.1093/jxb/erj175>.
- Begara-Morales, J.C., Chaki, M., Valderrama, R., Sánchez-Calvo, B., Mata-Pérez, C., Padilla, M.N., Barroso, J.B., 2018. Nitric oxide buffering and conditional nitric oxide release in stress response. *JXB* 69 (14), 3425–3438. <https://doi.org/10.1093/jxb/ery072>.
- Bertrand, M., Simonin, S., Bach, B., 2024. Applications of chitosan in the agri-food sector: a review. *Carbohydr. Res.*, 109219 <https://doi.org/10.1016/j.carres.2024.109219>.
- Bradford, M.M., 1976. A rapid and sensitive method for the quantitation of microgram quantities of protein utilizing the principle of protein-dye binding. *Anal. Biochem.* 72 (1–2), 248–254. [https://doi.org/10.1016/0003-2697\(76\)90527-3](https://doi.org/10.1016/0003-2697(76)90527-3).
- Campbell, W.H., 1999. Nitrate reductase structure, function and regulation: bridging the gap between biochemistry and physiology. *Annu. Rev. Plant Biol.* 50 (1), 277–303. <https://doi.org/10.1146/annurev.arplant.50.1.277>.
- Cao, Y., Lou, Y., Han, Y., Shi, J., Wang, Y., Wang, W., Ming, F., 2011. Al toxicity leads to enhanced cell division and changed photosynthesis in *Oryza rufipogon* L. *Mol. Biol. Rep.* 38, 4839–4846. <https://doi.org/10.1007/s11033-010-0618-9>.
- Cardozo, V.F., Lancheros, C.A., Narciso, A.M., Valereto, E.C., Kobayashi, R.K., Seabra, A.B., Nakazato, G., 2014. Evaluation of antibacterial activity of nitric oxide-releasing polymeric particles against *Staphylococcus aureus* and *Escherichia coli* from bovine mastitis. *Int. J. Pharm.* 473 (1–2), 20–29. <https://doi.org/10.1016/j.ijpharm.2014.06.051>.
- Chamizo-Ampudia, A., Sanz-Luque, E., Llamas, A., Galvan, A., Fernandez, E., 2017. Nitrate reductase regulates plant nitric oxide homeostasis. *Trends Plant Sci.* 22 (2), 163–174. <https://doi.org/10.1016/j.tplants.2016.12.001>.
- Chandra, S., Chakraborty, N., Dasgupta, A., Sarkar, J., Panda, K., Acharya, K., 2015. Chitosan nanoparticles: a positive modulator of innate immune responses in plants. *Sci. Rep.* 5 (1), 15195. <https://doi.org/10.1038/srep15195>.
- Chen, F., Wang, C., Yue, L., Zhu, L., Tang, J., Yu, X., Wang, Z., 2021. Cell walls are remodeled to alleviate nY₂O₃ cytotoxicity by elaborate regulation of *de novo* synthesis and vesicular transport. *ACS Nano* 15 (8), 13166–13177. <https://doi.org/10.1021/acsnano.1c02715>.
- Corpas, F.J., Carreras, A., Esteban, F.J., Chaki, M., Valderrama, R., Del Río, L.A., Barroso, J.B., 2008. Localization of S-nitrosothiols and assay of nitric oxide synthase and S-nitrosoglutathione reductase activity in plants. *Methods Enzymol.* 437, 561–574. [https://doi.org/10.1016/S0076-6879\(07\)37028-6](https://doi.org/10.1016/S0076-6879(07)37028-6).
- Corpas, F.J., González-Gordo, S., Palma, J.M., 2021. Nitric oxide and hydrogen sulfide modulate the NADPH-Generating enzymatic system in higher plants. *J. Exp. Bot.* 72 (3), 830–847. <https://doi.org/10.1093/jxb/eraa440>.
- Corpas, F.J., Taboada, J., Sánchez-Romera, B., López-Jaramillo, J., Palma, J.M., 2025. Peroxisomal sulfite oxidase (SOX), an alternative source of NO in higher plants which is upregulated by H₂S. *Plant Physiol. Biochem.* 225, 110000. <https://doi.org/10.1016/j.plaphy.2025.110000>.
- Dent, M.R., DeMartino, A.W., 2023. Nitric oxide and thiols: chemical biology, signalling paradigms and vascular therapeutic potential. *Br. J. Pharmacol.* <https://doi.org/10.1111/bph.16274>.
- do Carmo, G.C., Iastrenski, L.F., Debiassi, T.V., da Silva, R.C., Gomes, D.G., Pelegrino, M.T., Oliveira, H.C., 2021. Nanoencapsulation improves the protective effects of a nitric oxide donor on drought-stressed *Heliconia popayanensis* seedlings. *Ecotoxicol. Environ. Saf.* 225, 112713. <https://doi.org/10.1016/j.ecoenv.2021.112713>.
- Durand, C., Vicré-Gibouin, M., Follet-Gueye, M.L., Duponchel, L., Moreau, M., Lerouge, P., Driouch, A., 2009. The organization pattern of root border-like cells of *Arabidopsis* is dependent on cell wall homogalacturonan. *Plant Physiol.* 150 (3), 1411–1421. <https://doi.org/10.1104/pp.109.136382>.
- Gupta, K.J., Hancock, J.T., Petrivalsky, M., Kolbert, Z., Lindermayr, C., Durner, J., Loake, G.J., 2020. Recommendations on terminology and experimental best practice associated with plant nitric oxide research. *New Phytol.* 225 (5), 1828–1834. <https://doi.org/10.1111/nph.16157>.
- Hogg, N., 2002. The biochemistry and physiology of S-nitrosothiols. *Annu. Rev. Pharmacol.* 42 (1), 585–600. <https://doi.org/10.1146/annurev.pharmtox.42.092501.104328>.
- Ji, H., Wang, J., Chen, F., Fan, N., Wang, X., Xiao, Z., Wang, Z., 2022. Meta-analysis of chitosan-mediated effects on plant defense against oxidative stress. *Sci. Total Environ.* 851, 158212. <https://doi.org/10.1016/j.scitotenv.2022.158212>.
- Kacziba, B., Szierer, Á., Mészáros, E., Rónavári, A., Kónya, Z., Feigl, G., 2023. Exploration of signaling molecules in monocotyledonous crops with different CuO nanoparticle tolerance. *Plant Stress*, 100145. <https://doi.org/10.1016/j.stress.2023.100145>.
- Khan, M.N., 2024. S-nitrosoglutathione-facilitated activation of ATP synthase involves hydrogen sulfide during the response of plants to cadmium toxicity. *South Afr. J. Bot.* 165, 176–187. <https://doi.org/10.1016/j.sajb.2023.12.033>.
- Kneeshaw, S., Gelineau, S., Tada, Y., Loake, G.J., Spoel, S.H., 2014. Selective protein denitrosylation activity of Thioredoxin-h5 modulates plant immunity. *Mol. Cell* 56, 153–162. <https://doi.org/10.1016/j.molcel.2014.08.003>.
- Kolbert, Z., Pető, A., Lehotai, N., Feigl, G., Ördög, A., Erdei, L., 2012. *In Vivo* and *In Vitro* studies on fluorophore-specificity. *Acta Biol. Szeged.* 56, 37–41.
- Kolbert, Z., Feigl, G., Bordé, A., Molnár, Á., Erdei, L., 2017. Protein tyrosine nitration in plants: present knowledge, computational prediction and future perspectives. *Plant Physiol. Biochem.* 113, 56–63. <https://doi.org/10.1016/j.plaphy.2017.01.028>.
- Kolbert, Z., Molnár, Á., Szöllösi, R., Feigl, G., Erdei, L., Ördög, A., 2018. Nitro-oxidative stress correlates with Se tolerance of *Astragalus* species. *Plant Cell Physiol.* 59 (9), 1827–1843. <https://doi.org/10.1093/pcp/pcy099>.
- Kolbert, Z., Barroso, J.B., Brouquisse, R., Corpas, F.J., Gupta, K.J., Lindermayr, C., Hancock, J.T., 2019. A forty year journey: the generation and roles of NO in plants. *Nitric Oxide* 93, 53–70. <https://doi.org/10.1016/j.niox.2019.09.006>.
- Kolbert, Z., Barroso, J.B., Boscarì, A., Corpas, F.J., Gupta, K.J., Hancock, J.T., Loake, G.J., 2024. Interorgan, intraorgan and interplant communication mediated by nitric oxide and related species. *New Phytol.* 244 (3), 786–797. <https://doi.org/10.1111/nph.20085>.
- Kovacs, I., Holzmeister, C., Wirtz, M., Geerlof, A., Fröhlich, T., Römmling, G., Lindermayr, C., 2016. ROS-Mediated inhibition of S-nitrosoglutathione reductase contributes to the activation of anti-oxidative mechanisms. *Front. Plant Sci.* 7, 1669. <https://doi.org/10.3389/fpls.2016.01669>.
- Kurczyńska, E., Godel-Jedrychowska, K., Sala, K., Milewska-Hendel, A., 2021. Nanoparticles—Plant interaction: what we know, where we are? *Appl. Sci.* 11 (12), 5473. <https://doi.org/10.3390/app11125473>.
- Lehotai, N., Kolbert, Z., Pető, A., Feigl, G., Ördög, A., Kumar, D., Erdei, L., 2012. Selenite-induced hormonal and signalling mechanisms during root growth of *Arabidopsis thaliana* L. *J. Exp. Bot.* 63 (15), 5677–5687. <https://doi.org/10.1093/jxb/ers222>.
- León, J., 2022. Protein tyrosine nitration in plant nitric oxide signaling. *Front. Plant Sci.* 13, 859374. <https://doi.org/10.3389/fpls.2022.859374>.
- Li, R., He, J., Xie, H., Wang, W., Bose, S.K., Sun, Y., Yin, H., 2019. Effects of chitosan nanoparticles on seed germination and seedling growth of wheat (*Triticum aestivum* L.). *Int. J. Biol. Macromol.* 126, 91–100. <https://doi.org/10.1016/j.ijbiomac.2018.12.118>.
- Li, N., Lin, Z., Yu, P., Zeng, Y., Du, S., Huang, L.J., 2023. The multifarious role of callose and callose synthase in plant development and environment interactions. *Front. Plant Sci.* 14, 1183402. <https://doi.org/10.3389/fpls.2023.1183402>.
- Lopes-Oliveira, P.J., Gomes, D.G., Pelegrino, M.T., Bianchini, E., Pimenta, J.A., Stolf-Moreira, R., Oliveira, H.C., 2019. Effects of nitric oxide-releasing nanoparticles on neotropical tree seedlings submitted to acclimation under full sun in the nursery. *Sci. Rep.* 9 (1), 17371. <https://doi.org/10.1038/s41598-019-54030-3>.
- López-Gómez, P., Buezo, J., Urra, M., Cornejo, A., Esteban, R., de los Reyes, J.F., Urarte, E., Rodríguez-Dobrea, E., Chamizo-Ampudia, A., Eguaras, A., Wolf, S., 2024. A new oxidative pathway of nitric oxide production from oximes in plants. *Mol. Plant* 17, P178–P198. <https://doi.org/10.1016/j.molp.2023.12.009>.
- Ma, Y., Fu, L., Hussain, Z., Huang, D., Zhu, S., 2019. Enhancement of storability and antioxidant systems of sweet cherry fruit by nitric oxide-releasing chitosan nanoparticles (GSNO-CS NPs). *Food Chem.* 285, 10–21. <https://doi.org/10.1016/j.foodchem.2019.01.156>.
- Ma, M., Wendehenne, D., Philippot, L., Hänsch, R., Fletmetakis, E., Hu, B., Rennenberg, H., 2020. Physiological significance of pedospheric nitric oxide for root growth, development and organismic interactions. *Plant Cell Environ.* 43, 2336–2354. <https://doi.org/10.1111/pce.13850>.
- Martínez-Ruiz, A., Lamas, S., 2007. Signalling by NO-induced protein S-nitrosylation and S-glutathionylation: convergences and divergences. *Cardiovasc. Res.* 75 (2), 220–228. <https://doi.org/10.1016/j.cardiores.2007.03.016>.
- Matamoras, M.A., Cutrona, M.C., Wienkoop, S., Begara-Morales, J.C., Sandal, N., Orera, I., Becana, M., 2020. Altered plant and nodule development and protein S-nitrosylation in *Lotus japonicus* mutants deficient in S-nitrosoglutathione reductases. *Plant Cell Physiol.* 61 (1), 105–117. <https://doi.org/10.1093/pcp/pcz182>.
- Meilhoc, E., Boscarì, A., Bruand, C., Puppo, A., Brouquisse, R., 2011. Nitric oxide in legume-rhizobium symbiosis. *Plant Sci.* 181, 573–581. <https://doi.org/10.1016/j.plantsci.2011.04.007>.
- Methela, N.J., Islam, M.S., Lee, D.S., Yun, B.W., Mun, B.G., 2023a. S-Nitrosoglutathione (GSNO)-mediated lead detoxification in soybean through the regulation of ROS and metal-related transcripts. *Int. J. Mol. Sci.* 24 (12), 9901. <https://doi.org/10.3390/ijms24129901>.
- Methela, N.J., Pande, A., Islam, M.S., Rahim, W., Hussain, A., Lee, D.S., Yun, B.W., 2023b. Chitosan-GSNO nanoparticles: a positive modulator of drought stress tolerance in soybean. *BMC Plant Biol.* 23 (1), 639. <https://doi.org/10.1186/s12870-023-04640-x>.

- Milewska-Hendel, A., Sala, K., Gepfert, W., Kurczyńska, E., 2021. Gold nanoparticles-induced modifications in cell wall composition in barley roots. *Cells* 10 (8), 1965. <https://doi.org/10.3390/cells10081965>.
- Mohn, M.A., Thaqi, B., Fischer-Schrader, K., 2019. Isoform-specific NO synthesis by *Arabidopsis thaliana* nitrate reductase. *Plants* 8 (3), 67. <https://doi.org/10.3390/plants8030067>.
- Noorbakhsh, Z., Taheri, P., 2016. Nitric oxide: a signaling molecule which activates cell wall-associated defense of tomato against *Rhizoctonia solani*. *Eur. J. Plant Pathol.* 144, 551–568. <https://doi.org/10.1007/s10658-015-0794-5>.
- Oliveira, H.C., Gomes, B.C., Pelegrino, M.T., Seabra, A.B., 2016. Nitric oxide-releasing chitosan nanoparticles alleviate the effects of salt stress in maize plants. *Nitric Oxide* 61, 10–19. <https://doi.org/10.1016/j.niox.2016.09.010>.
- Pelegrino, M.T., Weller, R.B., Chen, X., Bernardes, J.S., Seabra, A.B., 2017. Chitosan nanoparticles for nitric oxide delivery in human skin. *Med Chem Comm* 8 (4), 713–719. <https://doi.org/10.1039/C6MD00502K>.
- Pelegrino, M.T., de Araujo, D.R., Seabra, A.B., 2018. S-nitrosoglutathione-containing chitosan nanoparticles dispersed in pluronic F-127 hydrogel: potential uses in topical applications. *Int J Drug Deliv Technol* 43, 211–220. <https://doi.org/10.1016/j.jddst.2017.10.016>.
- Pereira, A.E.S., Narciso, A.M., Seabra, A.B., Fraceto, L.F., 2015. Evaluation of the Effects of Nitric oxide-releasing Nanoparticles on Plants, 617. JPCS. IOP Publishing, p. 1. <https://doi.org/10.1088/1742-6596/617/1/012025>.
- Popova, E.V., Zorin, I.M., Domnina, N.S., Novikova, I.I., Krasnobaeva, I.L., 2020. Chitosan-tripolyphosphate nanoparticles: synthesis by the ionic gelation method, properties, and biological activity. *Russ. J. Gen. Chem.* 90, 1304–1311. <https://doi.org/10.1134/S1070363220070178>.
- Rockel, P., Strube, F., Rockel, A., Wildt, J., Kaiser, W.M., 2002. Regulation of nitric oxide (NO) production by plant nitrate reductase *In Vivo* and *In Vitro*. *J. Exp. Bot.* 53 (366), 103–110. <https://doi.org/10.1093/jexbot/53.366.103>.
- Rogers, L.A., Dubos, C., Surman, C., Willmet, J., Cullis, I.F., Mansfield, S.D., Campbell, M.M., 2005. Comparison of lignin deposition in three ectopic lignification mutants. *New Phytol.* 168 (1), 123–140. <https://doi.org/10.1111/j.1469-8137.2005.01496.x>.
- Saini, D., Bapatla, R.B., Vemula, C.K., Gahir, S., Bharath, P., Gupta, K.J., Raghavendra, A. S., 2024. Moderate modulation by S-nitrosoglutathione of photorespiratory enzymes in pea (*Pisum sativum*) leaves, compared to the strong effects of high light. *Protoplasma* 261, 43–51. <https://doi.org/10.1007/s00709-023-01878-y>.
- Sakamoto, A., Ueda, M., Morikawa, H., 2002. *Arabidopsis* glutathione-dependent formaldehyde dehydrogenase is an S-nitrosoglutathione reductase. *FEBS Lett.* 515 (1–3), 20–24. [https://doi.org/10.1016/S0014-5793\(02\)02414-6](https://doi.org/10.1016/S0014-5793(02)02414-6).
- Scarpin, D., Nerva, L., Chitarra, W., Moffa, L., D'Este, F., Vuerich, M., Petrusa, E., 2023. Characterisation and functionalisation of chitosan nanoparticles as carriers for double-stranded RNA (dsRNA) molecules towards sustainable crop protection. *Biosci. Rep.* 43 (11), BSR20230817. <https://doi.org/10.1042/BSR20230817>.
- Seabra, A.B., Silveira, N.M., Ribeiro, R.V., Pieretti, J.C., Barroso, J.B., Corpas, F.J., Oliveira, H.C., 2022. Nitric oxide-releasing nanomaterials: from basic research to potential biotechnological applications in agriculture. *New Phytol.* 234 (4), 1119–1125. <https://doi.org/10.1111/nph.18073>.
- Shah, S.U., Socha, M., Sejjil, C., Gibaud, S., 2017. Spray-dried microparticles of glutathione and S-nitrosoglutathione based on eudragit® FS 30D polymer. *Ann. Pharm. Fr.* 75 (2), 95–104. <https://doi.org/10.1016/j.pharma.2016.09.001>.
- Silveira, N.M., Seabra, A.B., Marcos, F.C., Pelegrino, M.T., Machado, E.C., Ribeiro, R.V., 2019. Encapsulation of S-nitrosoglutathione into chitosan nanoparticles improves drought tolerance of sugarcane plants. *Nitric Oxide* 84, 38–44. <https://doi.org/10.1016/j.niox.2019.01.004>.
- Silveira, N.M., Prativiera, P.J., Pieretti, J.C., Seabra, A.B., Almeida, R.L., Machado, E.C., Ribeiro, R.V., 2021. Chitosan-encapsulated nitric oxide donors enhance physiological recovery of sugarcane plants after water deficit. *EEB* 190, 104593. <https://doi.org/10.1016/j.envexpbot.2021.104593>.
- Sousa, B.T., Carvalho, L.B., Preisler, A.C., Saraiva-Santos, T., Oliveira, J.L., Verri, Jr WA., Oliveira, H., 2024. Chitosan coating as a strategy to increase postemergent herbicidal efficiency and alter the interaction of nanoatrazine with *Bidens pilosa* plants. *ACS Appl. Mater. Interfaces.* <https://doi.org/10.1021/acsami.4c03800>.
- Sravani, B., Dalvi, S., Narute, T.K., 2023. Role of chitosan nanoparticles in combating fusarium wilt (*Fusarium oxysporum* F. Sp. *ciceri*) of chickpea under changing climatic conditions. *J. Phytopathol.* 171 (2–3), 67–81. <https://doi.org/10.1111/jph.13159>.
- Suarez-Fernandez, M., Marhuenda-Egea, F.C., Lopez-Moya, F., Arnao, M.B., Cabrera-Escribano, F., Nueda, M.J., Lopez-Llorca, L.V., 2020. Chitosan induces plant hormones and defenses in tomato root exudates. *Front. Plant Sci.* 11, 572087. <https://doi.org/10.3389/fpls.2020.572087>.
- Sun, X.D., Ma, J.Y., Feng, L.J., Duan, J.L., Xie, X.M., Zhang, X.H., Yuan, X.Z., 2023. Magnetite nanoparticle coating chemistry regulates root uptake pathways and iron chlorosis in plants. *Proc. Natl. Acad. Sci. USA* 120 (27), e2304306120. <https://doi.org/10.1073/pnas.2304306120>.
- Suwanchaikasem, P., Idnurm, A., Selby-Pham, J., Walker, R., Boughton, B.A., 2024. The impacts of chitosan on plant root systems and its potential to be used for controlling fungal diseases in agriculture. *J. Plant Growth Regul.* 1–22. <https://doi.org/10.1007/s00344-024-11356-1>.
- Szöllösi, R., Molnár, Á., Kondak, S., Kolbert, Z., 2020. Dual effect of nanomaterials on germination and seedling growth: stimulation vs. phytotoxicity. *Plants* 9 (12), 1745. <https://doi.org/10.3390/plants9121745>.
- Tichá, T., Lochman, J., Činčalová, L., Luhová, L., Petrivalský, M., 2017. Redox regulation of plant S-nitrosoglutathione reductase activity through post-translational modifications of cysteine residues. *BBCR (Biochem. Biophys. Res. Commun.)* 494 (1–2), 27–33. <https://doi.org/10.1016/j.bbrc.2017.10.090>.
- Treffon, P., Rossi, J., Gabellini, G., Trost, P., Zaffagnini, M., Vierling, E., 2021. Proteome profiling of a S-Nitrosoglutathione reductase (GSNOR) null mutant reveals that aldo-keto reductases form a new class of enzymes involved in nitric oxide homeostasis. *Front. Plant Sci.* 12, 787435. <https://doi.org/10.3389/fpls.2021.787435>.
- Wang, X., Hargrove, M.S., 2013. Nitric oxide in plants: the roles of ascorbate and hemoglobin. *PLoS One* 8 (12), e82611. <https://doi.org/10.1371/journal.pone.0082611>.
- Xiao, D., Duan, X., Zhang, M., Sun, T., Sun, X., Li, F., Wang, D., 2018. Changes in nitric oxide levels and their relationship with callose deposition during the interaction between soybean and soybean mosaic virus. *Plant Biol.* 20 (2), 318–326. <https://doi.org/10.1111/plb.12663>.
- Xin, Y., Chen, F., Lai, S., Yang, H., 2017. Influence of chitosan-based coatings on the physicochemical properties and pectin nanostructure of Chinese cherry. *Postharvest Biol. Technol.* 133, 64–71. <https://doi.org/10.1016/j.postharvbio.2017.06.010>.
- Xu, Y., Du, Y., 2003. Effect of molecular structure of chitosan on protein delivery properties of chitosan nanoparticles. *Int. J. Pharm.* 250 (1), 215–226. [https://doi.org/10.1016/S0378-5173\(02\)00548-3](https://doi.org/10.1016/S0378-5173(02)00548-3).
- Yan, F., Zhu, Y., Müller, C., Schubert, S., 2001. Adaptation of plasma membrane H⁺-ATPase of proteoid roots of white lupin (*Lupinus albus* L.) to phosphorus deficiency. *Plant Nutrition: Food Security and Sustainability of agro-ecosystems Through Basic and Applied Research*, pp. 186–187.
- Ye, J., Coulouris, G., Zaretskaya, I., Cutcutache, I., Rozen, S., Madden, T., 2012. Primer-BLAST: a tool to design target-specific primers for polymerase chain reaction. *BMC Bioinf.* 13, 134. <https://doi.org/10.1186/1471-2105-13-134>.
- Zagorchev, L., Seal, C.E., Kranner, I., Odjakova, M., 2013. A central role for thiols in plant tolerance to abiotic stress. *Int. J. Mol. Sci.* 14 (4), 7405–7432. <https://doi.org/10.3390/ijms14047405>.
- Zelko, I., Lux, A., Sterckeman, T., Martinka, M., Kollárová, K., Lišková, D., 2012. An easy method for cutting and fluorescent staining of thin roots. *Ann. Bot.* 110 (2), 475–478. <https://doi.org/10.1093/aob/mcs046>.
- Zhan, N., Wang, C., Chen, L., Yang, H., Feng, J., Gong, X., Ren, B., Wu, R., Mu, J., Li, Y., Liu, Z., 2018. S-nitrosylation targets GSNO reductase for selective autophagy during hypoxia responses in plants. *Mol. Cell* 5 (1), 142–154. <https://doi.org/10.1016/j.molcel.2018.05.024>, 71.
- Zhang, X., 2004. Real time and in vivo monitoring of nitric oxide by electrochemical Sensors—From dream to reality. *Front. Biosci.* 9 (3434–3446), 17.